Chapter 4

Intramolecular Charge Transfer Based Metallogels

4.1 INTRODUCTION

In chapter 3, we designed and synthesized a chiral low molecular weight ligand $H_4T^{\text{-L-tyr}}$ which upon subsequent addition of LiOH and $Zn(NO_3)_2$ produced a transparent fluorescent metallogel (**CPH**). The synthesized gel was well explored for nanofabrication of Au nanoparticles and their nanocatalytic application towards model reduction reaction of 4-nitrophenol. Inspired from previous chapter about chiral symmetric ligand and its gelation behavior, in this chapter, we again designed a symmetrical chiral L-tartaric acid-based ligand comprised of suitably placed donor and acceptor part which may induce intramolecular charge transfer with or without metal addition under suitable conditions followed by metallogelation.

Supramolecular materials, especially, metallogels obtained an ever-growing attention due to their various additional properties.[1-3] In addition, introduction of chirality in the gelator tunes its morphological and optical properties.[4] Furthermore, molecular engineering of gelators for incorporation of the donor–acceptor (D–A) units may lead to charge transfer (CT) which is accompanied by the appearance of highly colored gels.[5] CT gels have various applications as thermo-chromic and opto-electronic materials.[5]

During the recent past bi/tri-component assisted CT organic gels have been successfully synthesized *via* the D–A strategy, but with limited intermolecular CT between organic gelators.[6] Such intermolecular D–A interactions endorse the gelation behavior and improve the molecular functionality of components toward stable supramolecular assembly.[6,7] Remarkably, apart from all these advances, the successful synthesis of solitary metallogelators (one component) exhibiting intramolecular charge transfer (ICT) and gelation properties is still a challenge. It may be due to the difficulties in the structural design

of a CT gelator, as it should have both donor and acceptor sites together within a single molecule, along with the metal binding and gelation properties. Accepting the challenge, strategically, we have designed an L-tartaric acid based symmetrical chiral gelator, for which the donor –NH group is placed at a reasonable π-conjugation distance from the strong electron withdrawing $–NO_2$ group (D–π–A type). In addition, the $–NO_2$ moiety is not only important for ICT, but also for gelation because it enhances the dipole moment, and in turn, aggregation through cation–dipole interactions.[8]

Recently, M. Dubey *et,al.*, reported the synthesis of metallogels using enantiopure chiral ligands, which exhibited exceptional morphology, anomalous fluorescence and rheological properties.[9,10] Inspired by our earlier efforts, in this chapter, we incorporated an enantiopure chiral flexible core in between two aforesaid D–π–A units with an objective to tune the morphology from ordinary long range fibers to twisted fibers along with additional intramolecular charge transfer properties. Thus, by following the A–π–D-chiral-D–π–A molecular design strategy, we could be able to produce entirely newfangled chiral metallogels with intramolecular charge transfer properties. To the best of our knowledge, for the first time, we reported the homochiral ICT metallogelation triggered by an alkali base.

4.2 EXPERIMENTAL METHODS

4.2.1 Materials and physical methods

Common reagents and solvents were purchased from Merck, Qualigens, Avra or S.D. Fine Chem. Ltd, Mumbai, India, and used as received without further purification. The solvents were dried and distilled following standard procedures prior to their use. L-Tartaric acid, 2-nitrobenzaldehyde, 3-nitrobenzaldehyde and 4-hydroxybenzaldehyde were purchased from Avra Synthesis Pvt. Ltd, Hyderabad, India, and used as received.

Elemental analyses were acquired on an Exeter CHN Analyzer CE-440. FT-IR and electronic absorption spectra were obtained on a PerkinElmer Spectrum 100 and a Thermo scientific EVOLUTION 201 spectrophotometer, respectively. ^{1}H NMR spectra were obtained on a Bruker AVANCE III HD 500 spectrometer. Electrospray ionization mass (ESI-MS) spectra were recorded on a Waters (Micromass MS Technologies) Q-Tof Premier. SEM images and EDS were captured using a Carl Zeiss EVO/18 Research 2045 and an Oxford Instruments 5IN1000EDS, respectively. CD spectra were recorded on a JASCO instrument, Model J-815-150S. Experiments were performed by purging dry N_2 gas continuously at 15 L min ^{1} during data acquisition. Data were collected using a quartz cuvette with a path length of 1 mm between 200 and 400 nm. Powder XRD data were collected on a Rigaku SmartLab between angle 2θ = 5–80^{o}. Electrical conductivity of the solution was measured on a Eutech Instruments CON 5/TDS 5 conductivity meter. The instrument was calibrated with standard solution and molar conductance was measured in acetonitrile and found to be 4 ohm^{-1} cm^{2} mol^{-1}, which indicates the nonconductive solution.

4.2.2 Rheological study

Measurements were performed using a stress-controlled rheometer (Anton Paar Quality Control Rheometer RheolabQC instrument) equipped with stainless steel parallel plates (20 mm diameter, 0.5 mm gap). Experiments were carried out on freshly prepared gels (1% w/v). Linear viscoelastic regions of the gel samples were determined by measuring the storage modulus, G$^{'}$ (associated with energy storage), and the loss modulus, G$^{"}$ (associated with the loss of energy) as a function of stress amplitude (dynamic oscillatory frequency of 10 rad s^{-1}). The following tests were performed: increasing amplitude of oscillation up to 100% apparent strain on shear, time and frequency sweeps at 25 ^{o}C (20 min and from 0.1 to 10 rad

s^{-1}, respectively), and a heating run at 110 ^{o}C at a scan rate of 5 ^{o}C min^{-1}. All these measurements were conducted twice.

4.2.3 Theoretical calculation

Quantum chemical calculations have been performed using a hybrid version of DFT and Hartree–Fock (HF) methods namely the B3LYP TD-FC,[11] wherein the exchange energy from Becke's exchange functional is combined with exact energy from Hartree–Fock theory. Basis set normal has been used for C, H, N and O, which combines quasi-relativistic effective core potentials with a valence double basis-set.[12] The geometry optimization and frequency calculations (to verify a genuine minimum energy structure) were performed by using the Gaussian 09 program.[13]

4.2.4 X-ray crystallography

The crystal suitable for single crystal X-ray analyses for **3** was obtained by recrystallization in the presence of KOH in acetonitrile and water mixture. The crystal was mounted on a glass fiber. All geometric and intensity data for **3** were collected at room temperature using a Oxford Super Nova CCD diffractometer equipped with a fine focus 1.75 kW sealed tube Mo-Kα (λ = 0.71073 Å) X-ray source, with increasing ω (width of 0.3 per frame) at a scan speed of either 3 or 5 s per frame. The strategy for data collection was evaluated by using the CrysAlisPro CCD software. The data were collected by standard 'phi and omega' scan techniques and scaled and reduced using CrysAlisPro RED software. Absorption corrections were made using SADABS only as either kind of absorption did not help.[14] After initial solution and refinement with SHELXL, the final refinements were performed on a WinGX environment using SHELX97.[15,16] All non-hydrogen atoms were refined anisotropically. Wherever possible, the hydrogen atoms were located from the difference Fourier maps and

refined isotropically. Thus, some of the C–H bonds will not be ideal and may vary. Selected crystallographic data have been summarized in parentheses in Fig. 4.19.[17]

4.2.5 Synthetic procedure

4.2.5.1 Synthesis of 2,3-dihydroxysuccinohydrazide (A)

The precursor compound (**A**), gelators (structural isomers, ($H_2SI^{L\text{-}tart}$) (**1**), ($H_2SI^{L\text{-}tart}$) (**2**) and ($H_2SI^{L\text{-}tart}$) (**3**)) and ligand ($H_4L^{L\text{-}tart}$) (**4**) were synthesized by standard literature procedures with slight modifications.[9]

4.2.5.2 Synthesis of (10E,12E)-N1',N4'-bis(2-nitrobenzylidene)-2,3-dihydroxysuccinohydrazide ($H_2SI^{L\text{-}tart}$) (**1**). The precursor **A** (0.100 g, 0.56 mmol) was dissolved in distilled water (5 mL) and a methanolic solution of 2-nitrobenzaldehyde (0.166 g, 1.10 mmol, 10 mL) was added drop wise to it with continuous stirring at room temperature. The reaction mixture was stirred for additional 2 hours. It afforded a shiny pale yellow solid, which was filtered, washed thoroughly with water and diethyl ether, and dried under vacuum. Yield 0.185 g (76%). Anal. calcd for $C_{18}H_{16}N_6O_8$: C, 48.65; H, 3.63; N, 18.91. Found C, 48.83; H, 3.94; N, 18.73. ^{1}H NMR (500 MHz, DMSO-d_6, ppm): δ 4.53 (d, 2H, –CH), 5.99 (d, 2H, –OH), 7.72 (t, 2H, Ar), 8.12 (t, 2H, Ar), 8.20 (d, 2H, Ar), 8.48 (d, 2H, Ar), 8.58 (s, 2H, =CH), 11.49 (s, 2H, –NH). Due to poor solubility of the neutral form, ESI-MS was performed by dissolving the solid in acetonitrile in the presence of 4 equiv. of LiOH·H_2O. *m/z*, ESI-MS: $[M + Li]^+$, 451.11 (calcd 451.11); $[M–H]^–$, 443.1 (calcd 443.3). IR (KBr, cm^{-1}) $\upsilon\nu$(–OH) 3419, $\nu(NH)_{sym}$ 3251, ν(C=O) 1655 (s), 1527 (s). UV-vis spectrum (dimethyl sulfoxide) [λ_{max}, nm (ε, $M^{-1}cm^{-1}$)]: 292 (27 800).

4.2.5.3 Synthesis of (10E,12E)-N1',N4'-bis(3-nitrobenzylidene)-2,3-dihydroxysuccinohydrazide ($H_2SI^{L\text{-}tart}$) (**2**). It was synthesized following the above procedure described for **1**,

using 3-nitro-benzaldehyde instead of 2-nitrobenzaldehyde. Yield 0.210 g (86%). Anal. calcd for $C_{18}H_{16}N_6O_8$: C, 48.65; H, 3.63; N, 18.91. Found C, 48.76; H, 3.88; N, 18.58. ^{1}H NMR (500 MHz, DMSO-d_6, ppm): δ 4.51 (d, 2H, –CH), 5.92 (d, 2H, –OH), 7.66 (t, 2H, Ar), 7.79 (d, 2H, Ar), 8.04 (m, 4H, Ar), 8.83 (s, 2H, =CH), 11.67 (s, 2H, –NH). Due to poor solubility of the neutral form, ESI-MS was performed by dissolving the solid in acetonitrile in the presence of 4 equiv. of LiOH·H_2O. *m/z*, ESI-MS: $[M + Li]^+$, 451.45 (calcd 451.11). IR (KBr, cm^{-1}) $\nu(NH)_{sym}$ 3289, ν(C=O) 1673 (s), 1524 (s). UV-vis spectrum (dimethyl sulfoxide) [λ_{max}, nm (ε, $M^{-1}cm^{-1}$)]: 285 (38 100).

4.2.5.4 Synthesis of (10E,12E)-N1',N4'-bis(4-nitrobenzylidene)-2,3-dihydroxysuccinohydrazide($H_2SI^{L\text{-}tart}$) (3). It was also synthesized by following similar procedures described for **1** and **2**, using 4-nitrobenzaldehyde in place of 2 or 3-nitrobenzaldehyde. Yield 0.190 g (78%). Anal. calcd for $C_{18}H_{16}N_6O_8$: C, 48.65; H, 3.63; N, 18.91. Found C, 48.93; H, 3.61; N, 19.30. ^{1}H NMR (500 MHz, DMSO-d_6, ppm): δ 4.54 (s, 2H, –CH), 6.01 (s, 2H, –OH), 7.93 (d, 4H, Ar), 8.29 (d, 4H, Ar), 8.58 (s, 2H, =CH), 11.56 (s, 2H, –NH). Due to poor solubility of the neutral form, ESI-MS was performed by dissolving the solid in acetonitrile in the presence of 4 equiv. of LiOH·H_2O. *m/z,* ESI-MS: $[M + Li]^+$, 451.47 (calcd 451.11); $[M–H]^–$, 443.4 (calcd 443.3). IR (KBr, cm^{-1}) ν(–OH) 3428, $\nu(NH)_{sym}$ 3228, ν(C=O) 1673 (s), 1514 (s). UV-vis spectrum (dimethyl sulfoxide) [λ_{max}, nm (ε, $M^{-1}cm^{-1}$)]: 337 (51 200).

Note: The pale-yellow colored crystals of isomer **3** were obtained from the intense yellow colored solution of **3** and KOH (1:4) in the acetonitrile and water mixture within 2–3 days.

4.2.5.5 Synthesis of (10E,12E)-N1',N4'-bis(4-carboxybenzylidene)-2,3-dihydroxysuccinohydrazide($H_4L^{L\text{-}tart}$) (4). It was synthesized by following the procedure described for **1**, using 4-formylbenzoic acid instead of 2-nitrobenzaldehyde. Yield 0.218 g (89%). Anal. calcd

for $C_{18}H_{16}N_6O_8$: C, 54.30; H, 4.10; N, 14.66. Found C, 54.46; H, 4.53; N, 13.01. ^{1}H NMR (500 MHz, DMSO-d_6, ppm): δ 4.51 (s, 2H, –CH), 5.95 (s, 2H, –OH), 7.77 (d, 4H, Ar), 7.99 (d, 4H, Ar), 8.50 (s, 2H, =CH), 11.38 (s, 2H, –NH), 14.75 (s, 2H, –COOH). Due to poor solubility of the neutral form, ESI-MS was performed by dissolving the solid in acetonitrile in the presence of 4 equiv. of LiOH·H_2O. *m/z*, ESI-MS: $[M + Li]^+$, 451.29 (calcd 451.11). IR (KBr, cm^{-1}) ν(–OH) 3397, $\nu(NH)_{sym}$ 3279, ν(C=O) 1686 (s), 1536 (s). UV-vis spectrum (dimethyl sulfoxide) [λ_{max}, nm (ε, $M^{-1}cm^{-1}$)]: 307 (50 100).

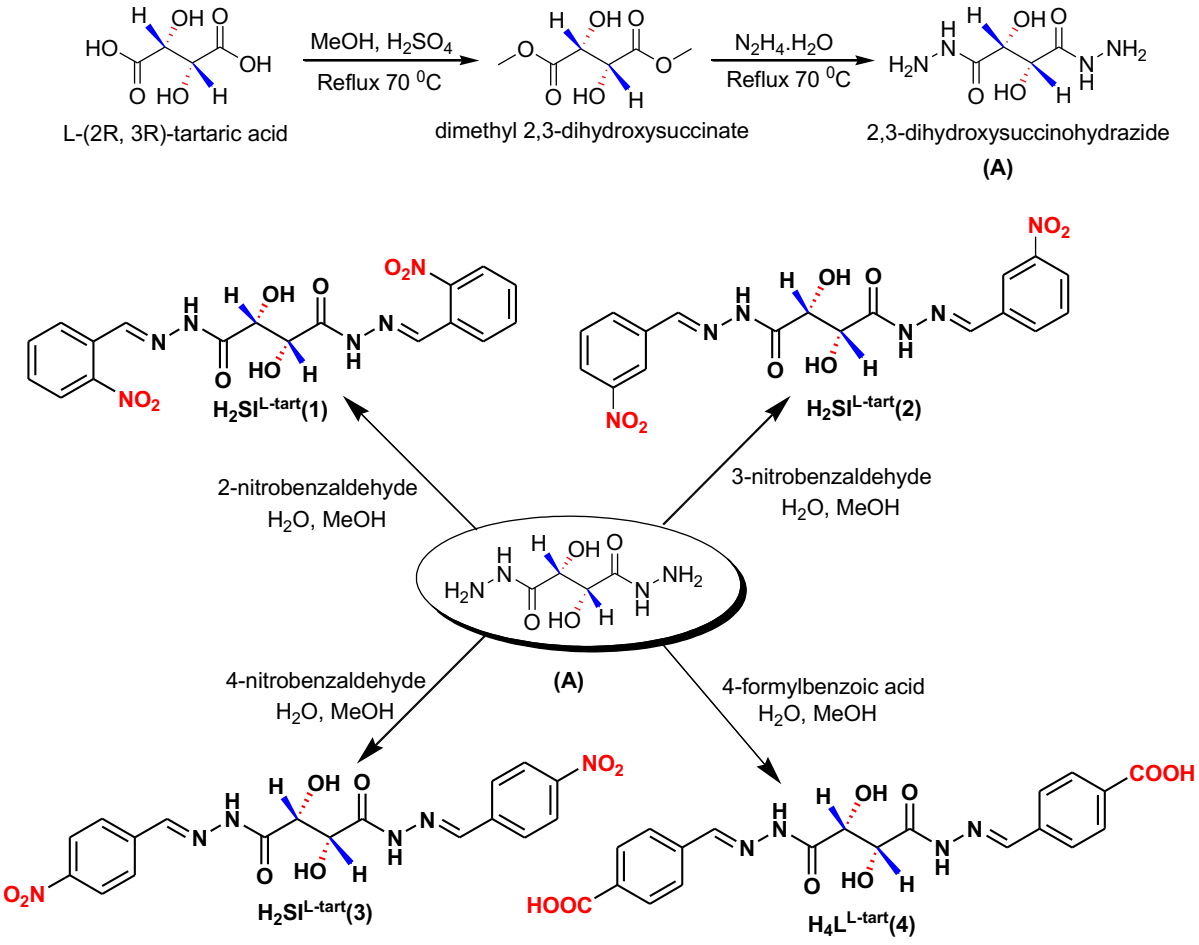

Scheme 4.1 A synthetic strategy adopted for the precursor **A**, structural isomers (SI **1**-**3**) and ligand (**4**)

4.3 RESULTS AND DISCUSSION

Three structural isomeric nitrobenzylidenes $H_2SI^{L\text{-}tart}$ (**1**–**3**) and carboxybenzylidene $H_4SI^{L\text{-}tart}$ (**4**) have been synthesized in reasonably good yield (Scheme 4.1).[9] Characterization data of these compounds well commensurate with their proposed formulations (section 4.2.5). They are insoluble in common solvents except DMSO. However, upon treatment with aqueous solutions of LiOH, NaOH, KOH and CsOH, they dissolved instantly and showed very interesting properties. The quick mixing of a pale yellow solution of **3** in DMSO with an aqueous solution of LiOH (1:4) produced an intense red colored gel (1% w/v), which was confirmed by an inverted vial method. The dark yellow colored gels were obtained using less polar solvents like acetone, acetonitrile, methanol and ethanol (Scheme 4.2). Furthermore, in the presence of bigger alkali bases like NaOH, KOH and CsOH, **3** produced transparent solution in all the common solvents under similar conditions. Notably, parallel gelation tests were performed with **1** and we found that both LiOH and NaOH form a colored gel (0.5% w/v) in acetonitrile and acetone only. Interestingly, **2** neither forms a gel nor produce any color change before and after the addition of LiOH in the aforesaid solvents under similar conditions (Table 4.1 and Scheme 4.2). Remarkably, gelation was not observed in the presence of other bases like tetrabutylammonium hydroxide (Bu_4NOH), ammonia and triethylamine indicating the vital role of the alkali metal ion in gelation. Furthermore, the thermal stability of the gel was established by heating the gel to 75 ^oC and cooling to room temperature. Notably, it increased upon heating and decreased upon cooling in a reversible manner rather than melting or drying (Fig. 4.2). Furthermore, the gel showed a significant color change upon heating and cooling in a reversible manner. The mechanical strength and

self-healing properties of the gel (**1** + Na^+, acetone) are demonstrated by cut and piece pick up experiments (Figure 4.1).

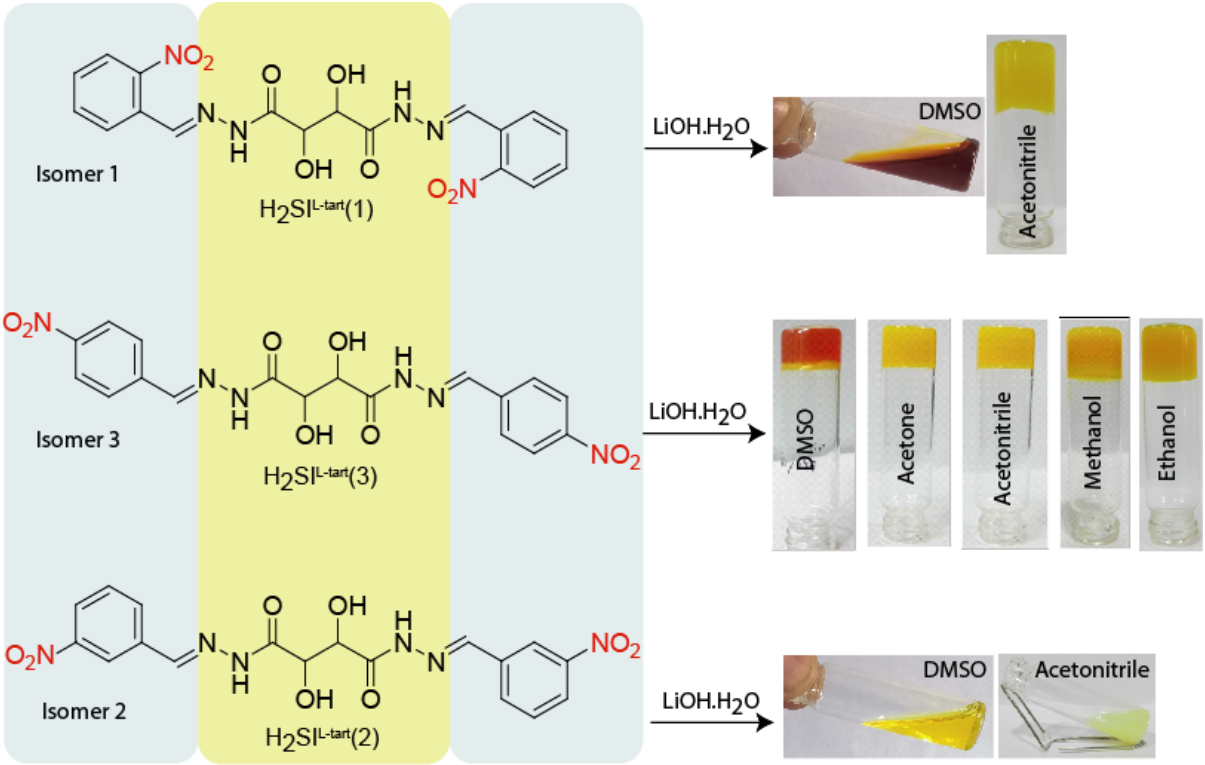

Scheme 4.2 A schematic representation of gelation property of structural isomers **1**-**3** in presence of LiOH in various solvents. Isomer **3** is preeminent candidate for gelation in DMSO, acetone, acetonitrile, methanol and ethanol. While the isomer **1** does not form gel in DMSO but shows the gelation in acetonitrile as well as in acetone. On the other hand, isomer **2** forms the solution or gelatinous precipitate in DMSO and acetonitrile.

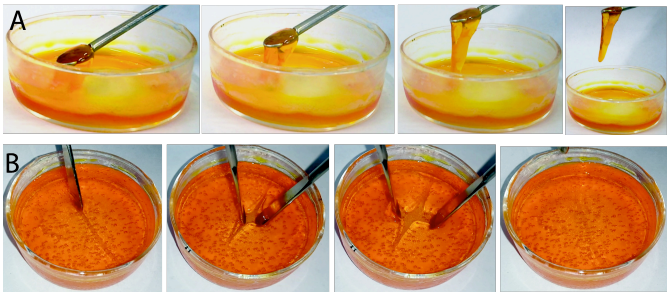

Figure 4.1 (A) Freshly prepared **1**+Li^+ containing gel in acetone in a Petri dish at 20 °C which can be lift up by spatula shows the mechanical strength of gel, **(B)** A cut experiment of gel demonstrate the partial self-healing property.

Table 4.1 Gelation details of isomer **1** and **2**

	Isomer 1				Isomer2		
	Li^+	Na^+	K^+	NEt_3/NH_3	Li^+	Na^+	K^+
DMSO	S	S	S	S	S	S	S
Acetonitrile	G	G	S	I	GP	S	S
Acetone	G	G	S	I	S	S	S
MeOH	S	S	S	I	S	S	S
Ethanol	S	S	S	I	S	S	S
Water	PS	PS	PS	I	PS	PS	PS

Table 4.2 Gelation details of isomer **3** and ligand **4***

	Isomer 3			Ligand 4		
	Li^+	Na^+	Li^+	Li^+	Na^+	Li^+
DMSO	G	S	G	G	S	G
Acetonitrile	G	S	G	G	S	G
Acetone	G	S	G	G	S	G
MeOH	G	S	G	G	S	G
Ethanol	G	S	G	G	S	G
Water	PS	PS	PS	PS	PS	PS

*Where, S= solution, G= gel, GP= gelatinous precipetate, PS= partially soluble and I= Insoluble

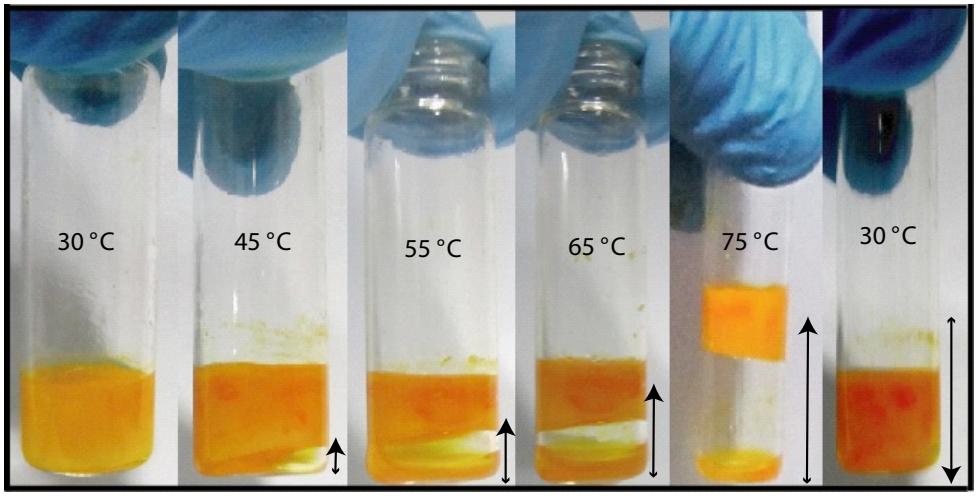

Figure 4.2 Acetonitrile containing gel (**1**+Li^+) in a vial inserted in water bath at 30 °C, gel started lifting up upon increasing the temperature and completely lifted at 75 °C. Notably, at 75 °C gel shows the distinct color change and after cooling exhibits the more intense red color than original gel. The experiment can be repeated more than 3 times. (The present gel is tight enough that the acetonitrile vapor cannot pass through the gel matrix resulted in the gel lifted up with the help of pressure created by acetonitrile vapor. This experiment indicates stability of gel at elevated temperature 75 °C.)

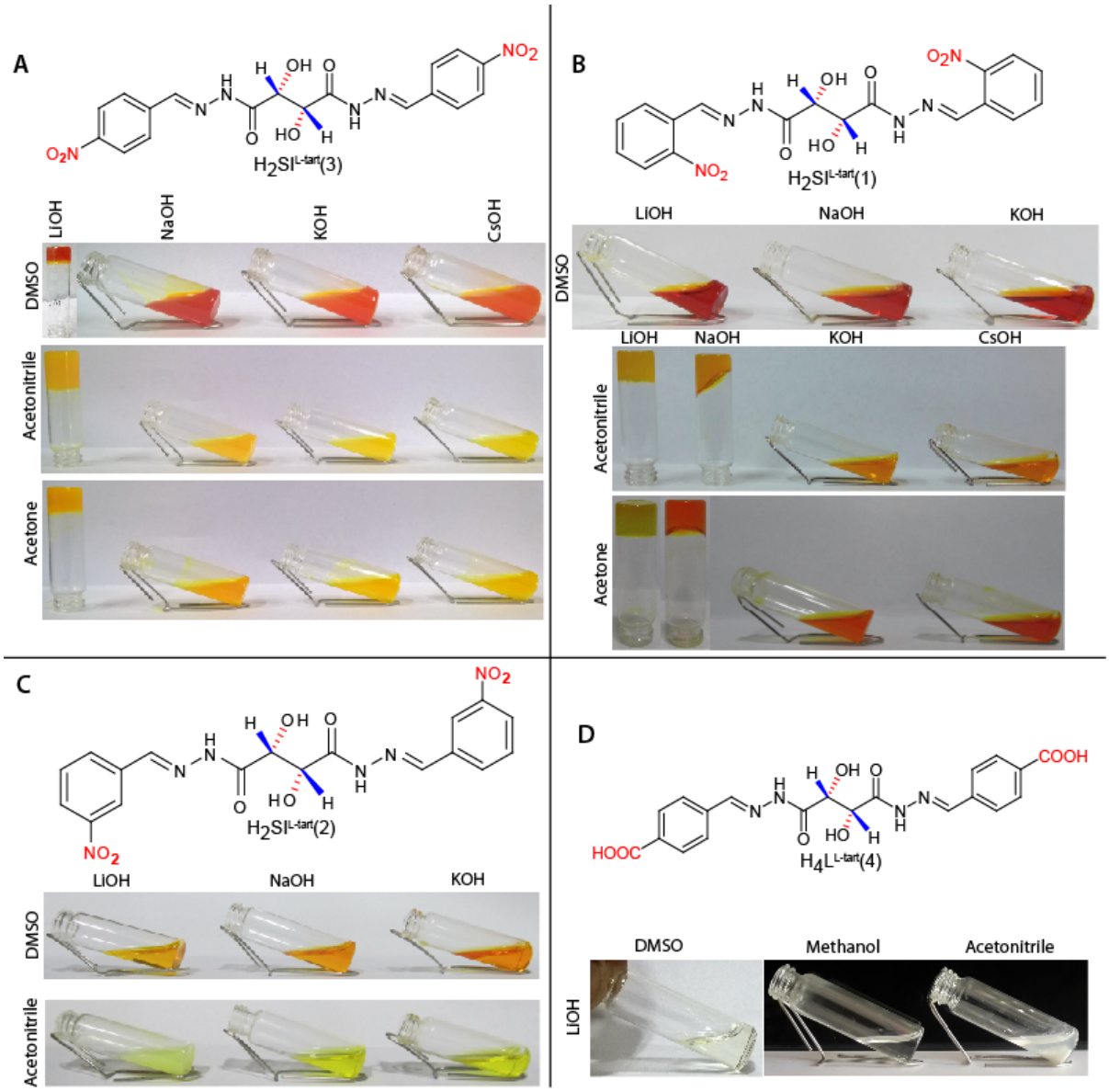

Figure 4.3 A complete summary of gelation property of isomers **1**-**3** and ligand **4** in various combinations of alkali base and solvent (A) Isomer **3**, (B) Isomer **1**, (C) Isomer **2** and (D) Isomer **4**. Isomer **2** neither form gel nor produce any intense color in comparison to isomer **1** and **3** while ligand **4** remain colorless after treatment with LiOH.

4.3.1 Morphological Characterization

The morphology of the gels was examined using a scanning electron microscope (SEM) directly on acetonitrile and acetone containing xerogels. Li^+ containing gels of **3** and **1** revealed articulate long range fibrous networks (Figure 4.4). Highlighting the results of the present work, **3** + Na^+ solution and **1** + Na^+ xerogel displayed marigold flower like and lucid

twisted morphology, respectively (Figure 4.4).[3,4] Thus, our factual target and the reason behind the introduction of chirality were obtained as twisted fibrous morphology. To avoid any artefact, we clearly state that more twisted fibers were obtained on the surface compared to deep layers may be due to different drying rates of a mixture of solvents. Furthermore, the formation of twisted fibers was attested by the SEM images of xerogels of acetone containing **1**+Na^+ gel (Figure 4.7). Furthermore, in the presence of bigger alkali metal ions like K^+ and Cs^+ crystal growth was obtained (Figure 4.6). Moreover, solution containing isomer **2**+Li^+/Na^+/K^+ revealed broken random fibrous morphology (Figure 4.8). Thus, the presence of aggregation cannot be ruled out in all the possible combinations of isomers and alkali metal ions, but the requisite extent of aggregation only directs the gelation. The effect of the size of alkali metal ions on gel or self-assembly processes has already been well explored previously.[10] Furthermore, chiral twist *via* metal ion induction has also been investigated.[18] The presence of alkali metal ions in their respective morphology was proved by energy dispersive X-ray (EDX) spectroscopy analysis (Figure 4.5). Thus, the overall morphological studies of various combinations of isomers and alkali metal ions exclusively support their gel and solution formation behavior.

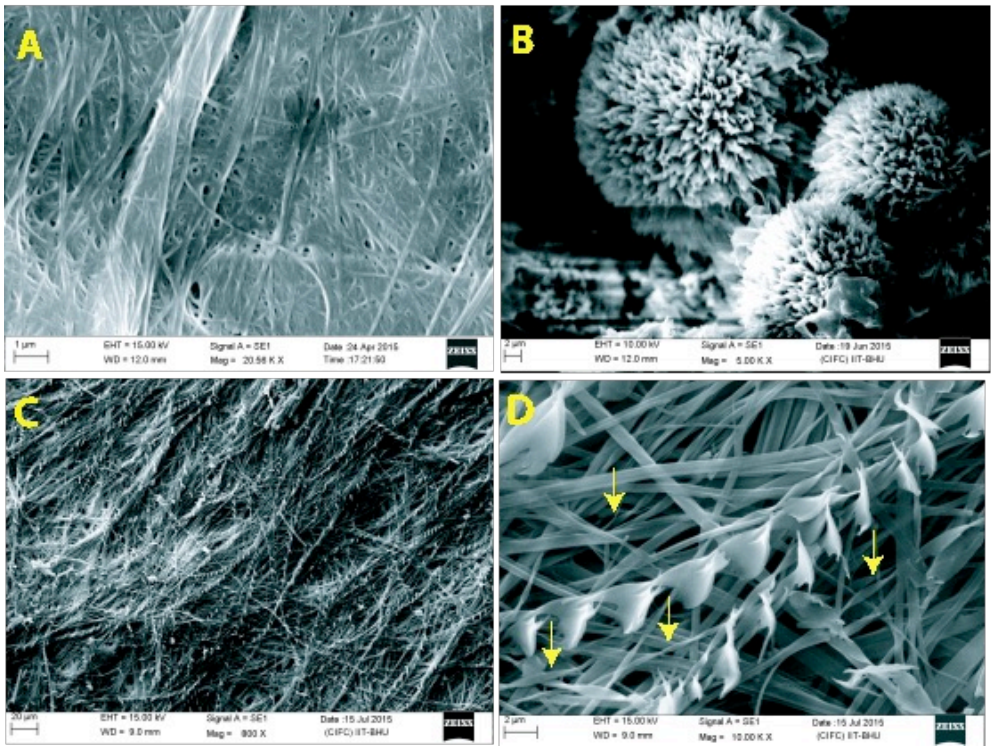

Figure 4.4 SEM images of xerogels or dried solution of (A) **3**+Li^+, (B) **3**+Na^+, (C) **1**+Na^+ showing the fibre, marigold and twisted fibrous morphology, respectively and (D) magnified image of C.

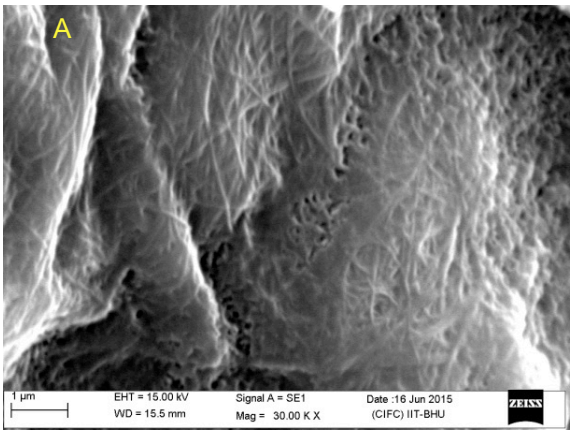
A
1 µm
EHT = 15.00 kV
WD = 15.5 mm
Signal A = SE1
Mag = 30.00 K X
Date :16 Jun 2015
(CIFC) IIT-BHU
ZEISS

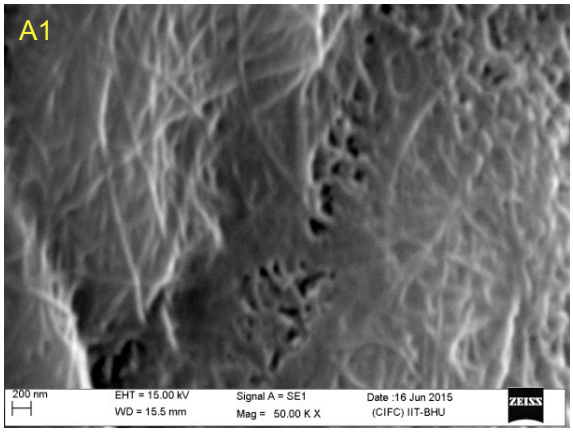
A1
200 nm
EHT = 15.00 kV
WD = 15.5 mm
Signal A = SE1
Mag = 50.00 K X
Date :16 Jun 2015
(CIFC) IIT-BHU
ZEISS

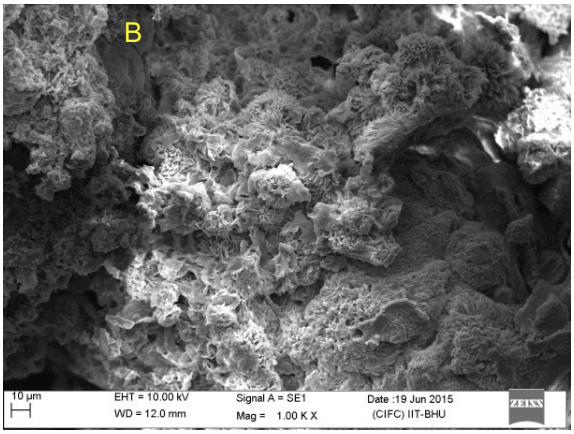
B
10 µm
EHT = 10.00 kV
WD = 12.0 mm
Signal A = SE1
Mag = 1.00 K X
Date :19 Jun 2015
(CIFC) IIT-BHU
ZEISS

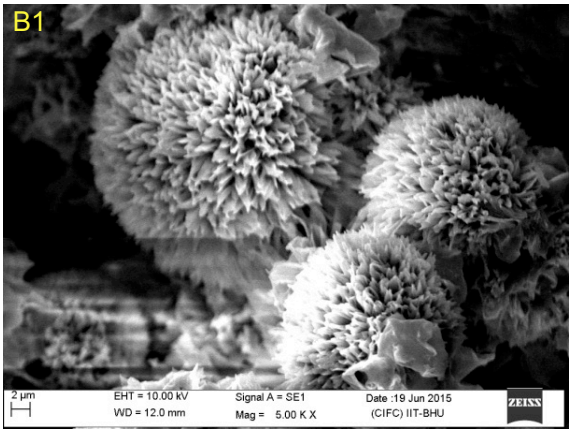
B1
2 µm
EHT = 10.00 kV
WD = 12.0 mm
Signal A = SE1
Mag = 5.00 K X
Date :19 Jun 2015
(CIFC) IIT-BHU
ZEISS

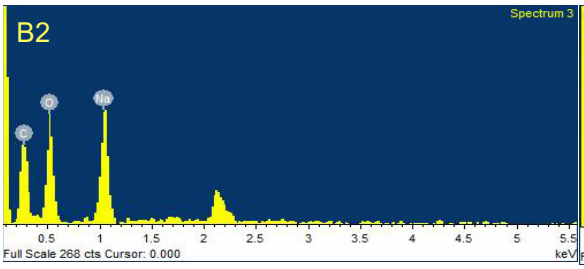
B2
Spectrum 3
O
Na
C
0.5
1
1.5
2
2.5
3
3.5
4
4.5
5
5.5
Full Scale 268 cts Cursor: 0.000
keV

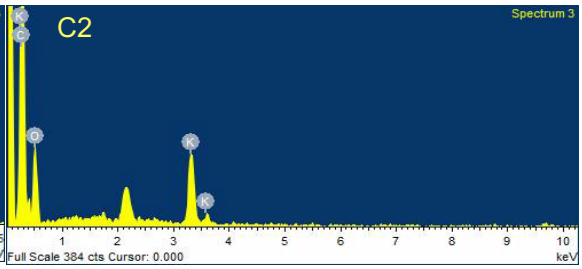
C2
Spectrum 3
K
C
O
K
K
1
2
3
4
5
6
7
8
9
10
Full Scale 384 cts Cursor: 0.000
keV

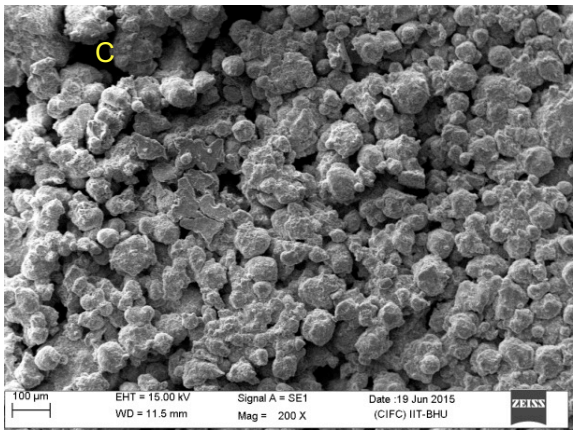
C
100 µm
EHT = 15.00 kV
WD = 11.5 mm
Signal A = SE1
Mag = 200 X
Date :19 Jun 2015
(CIFC) IIT-BHU
ZEISS

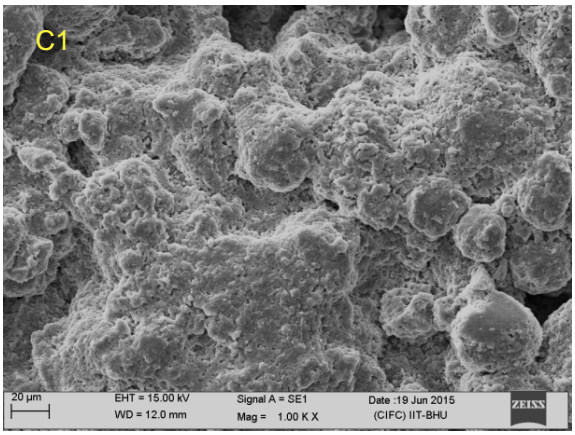
C1
20 µm
EHT = 15.00 kV
WD = 12.0 mm
Signal A = SE1
Mag = 1.00 K X
Date :19 Jun 2015
(CIFC) IIT-BHU
ZEISS

Figure 4.5 SEM images of isomer **3** and acetone containing dried gel/solution of showing the (A) well-ordered long range fibrous in presence of LiOH, (A1) magnified image of A, (B) unique flower like aggregated growth in presence of NaOH, (B1) magnified image of B, (B2) EDX of B1, (C2) EDX of C1, (C) crystal growth in presence of KOH and (C1) magnified image of C.

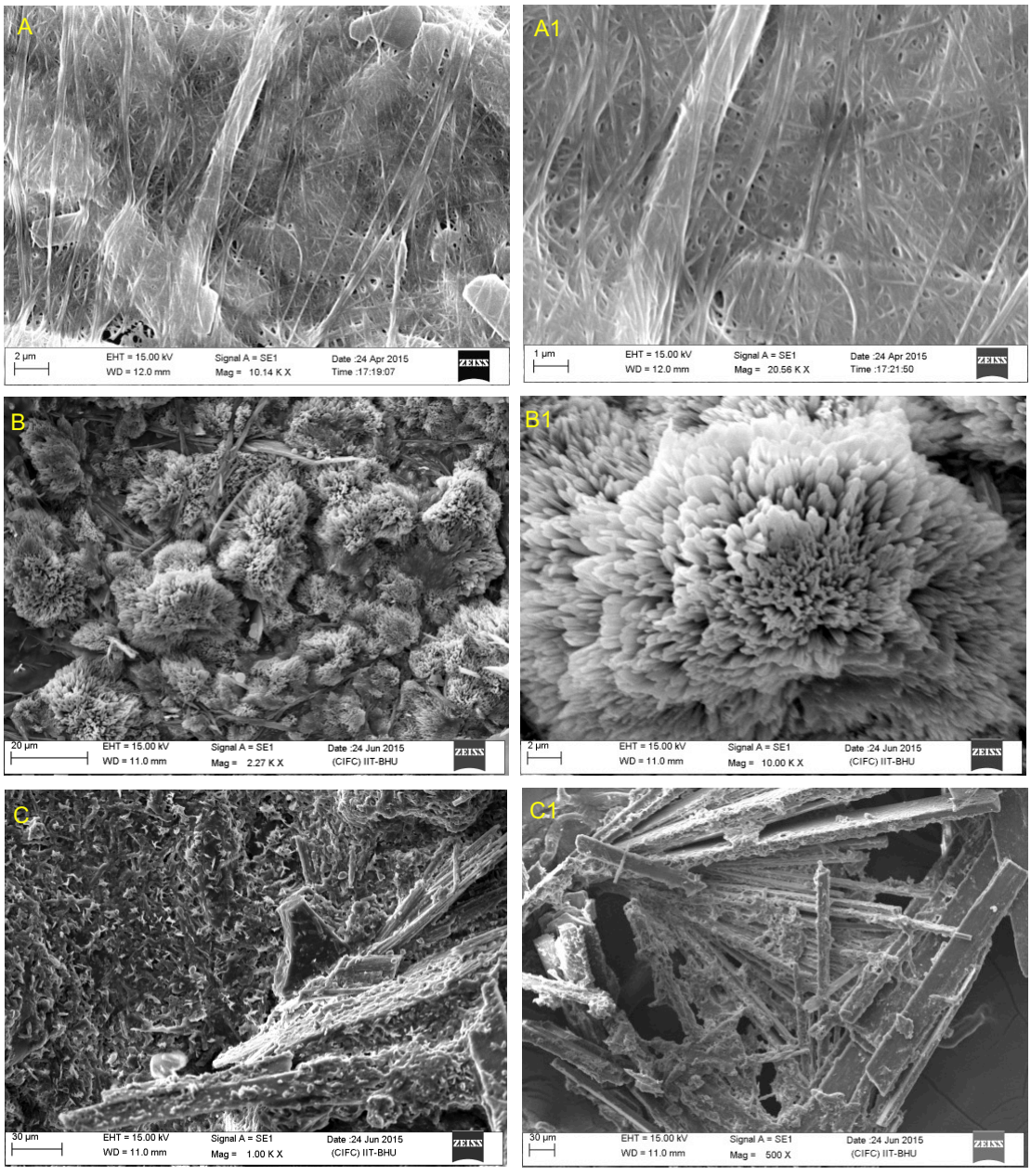

Figure 4.6 SEM images of isomer **3** and acetonitrile containing dried gel/solution well supports results shown in the figure 4.4 (A) well-ordered long range fibers in presence of LiOH, (A1) magnified image of A, (B) unique flower like aggregated growth in presence of NaOH, (B1) magnified image of B, (C) crystal growth in presence of KOH and (C1) magnified image of C.

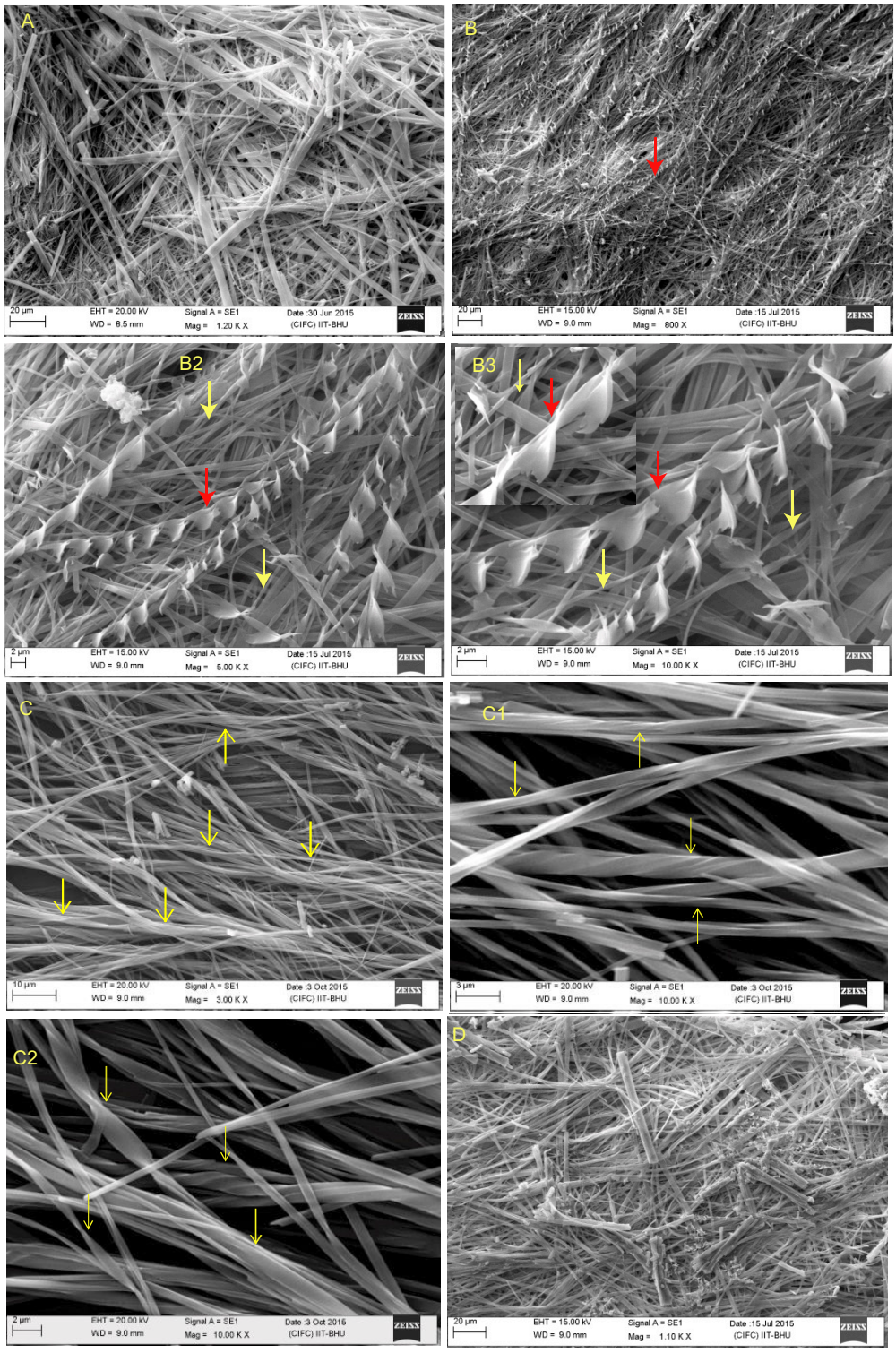

Figure 4.7 SEM images of isomer **1** and acetonitrile/acetone containing dried gel/solution (A) fibrous in presence of LiOH, (B) twisted fibrous morphology in presence of NaOH and acetonitrile, (B1), (B2) and (B3) magnified image of B, (C) twisted fibrous morphology of

xerogel of acetone containing gel, (C1) and (C2) magnified image of C (D) broken fibrous morphology in presence of KOH and (C1) magnified image of C.

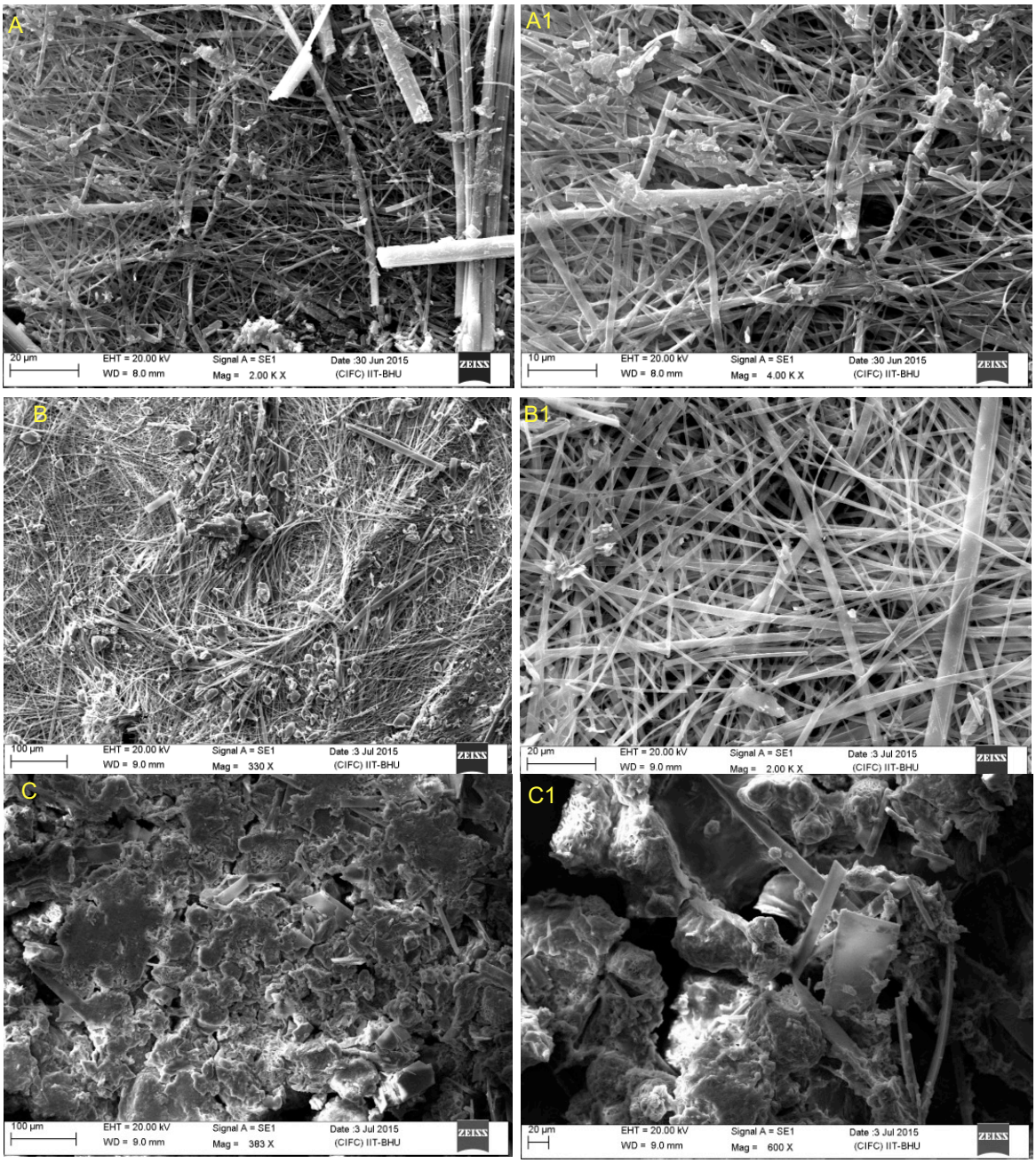

Figure 4.8 SEM images of isomer **2** and acetonitrile containing dried solution (A) broken fibers in presence of LiOH, (A1) magnified image of A, (B) random fibers in presence of NaOH, (B1) magnified image of B, (C) no conclusive morphology in presence of KOH and (C1) magnified image of C.

4.3.2 Circular Dichroism (CD) studies

Alkali metal ion dependent morphological diversity motivated us to perform circular dichroism (CD) studies on gels. The chiral nature of three isomers was characterized by CD in acetonitrile. The CD signals of isomer **3** + Li^+, **1** + Li^+ and **2** + Li^+ showed the positive Cotton effect at 390, 372 and 345 nm, respectively (Figure 4.9). Entirely different results obtained with **2** + Li^+ may be due to the absence of CT. The diluted gel of **1** + Li^+ ($5x10^{-4}$ M) exhibits a positive Cotton effect at 372, 312 and 265 nm, and a negative effect at 285 and 235 nm. Remarkably, upon alteration of Li^+ to Na^+, diluted gel (**1** + Na^+, $5x10^{-4}$ M) showed a negative Cotton effect at 390 nm instead of a positive Cotton effect at 372 nm, while other peaks followed a similar trend in both the cases (Figure 4.9). This Na^+ selective inversion of the CD signal strongly supports the chiral twisted morphology observed in **1** + Na^+ containing metallogels (Figure 4.4 and Figure 4.7). The inversion of the CD signal corresponding to CT peak only may be due to conformational changes involving the $–NO_2$ substituent affected by Na^+ selectively, which leads to twisted fiber formation.[19] Such Na^+ selective morphological tuning as well as inversion of the CD peak have not been reported for chiral low molecular weight metallogels.

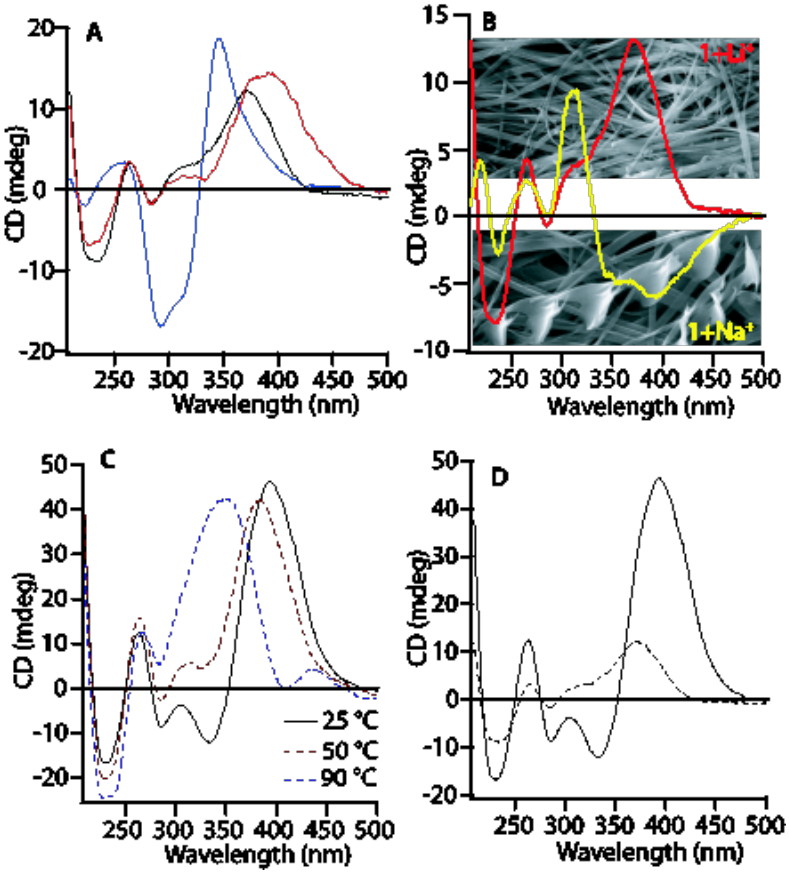

Figure 4.9 CD spectra of diluted gel in acetonitrile (A) **1** (black line), **2** (blue line) and **3** (red line) in presence of LiOH; (B) **1**+Li^+ (red line) and **1**+Na^+ (blue line) in acetonitrile ($5x10^{-4}$ M) shows the inversion of CT peak only; (C) **1**+Li^+ ($1x10^{-3}$ M) upon heating up to 90 ^{0}C shows blue shift of peak corresponding to CT only and (D) Diluted gel in acetonitrile (**1**+Li^+; conc. $1x10^{-3}$ M) in continuous line and further dilution in dotted line shows blue shift of peak corresponding to CT only.

4.3.3 UV-vis studies

An Isomer specific anomalous coloration and gelation have been investigated by UV-vis studies. A clear colorless solution of **3** displayed a sharp band at 337 nm (DMSO; $1x10^{-5}$ M; ε, 51 200 M^{-1} cm^{-1}) corresponding to the π–π* transition. Aliquot addition of LiOH to a solution of **3** led to a concomitant decrease in the absorbance of the band at 337 nm and the appearance of a new band at 457 nm ($\Delta\lambda$ = 120 nm) along with an isosbestic point at 377 nm (Fig. 4.10). This unique red shift upon addition of LiOH in a reasonable UV-vis region

indicates the formation of a CT complex. Furthermore, the formation of an intense red colored CT complex is not only triggered by Li^+, but also by Na^+, K^+, Cs^+ and Bu_4N^+ to the same extent (Fig. 4.10, Fig. 4.11 and Fig. 4.17). Remarkably, the color of the solution started to fade after 3 days, which also indicates the formation of an unstable CT complex. 1 displayed a less intense CT band at 443 nm under similar conditions indicating the importance of the position of the $–NO_2$ group.

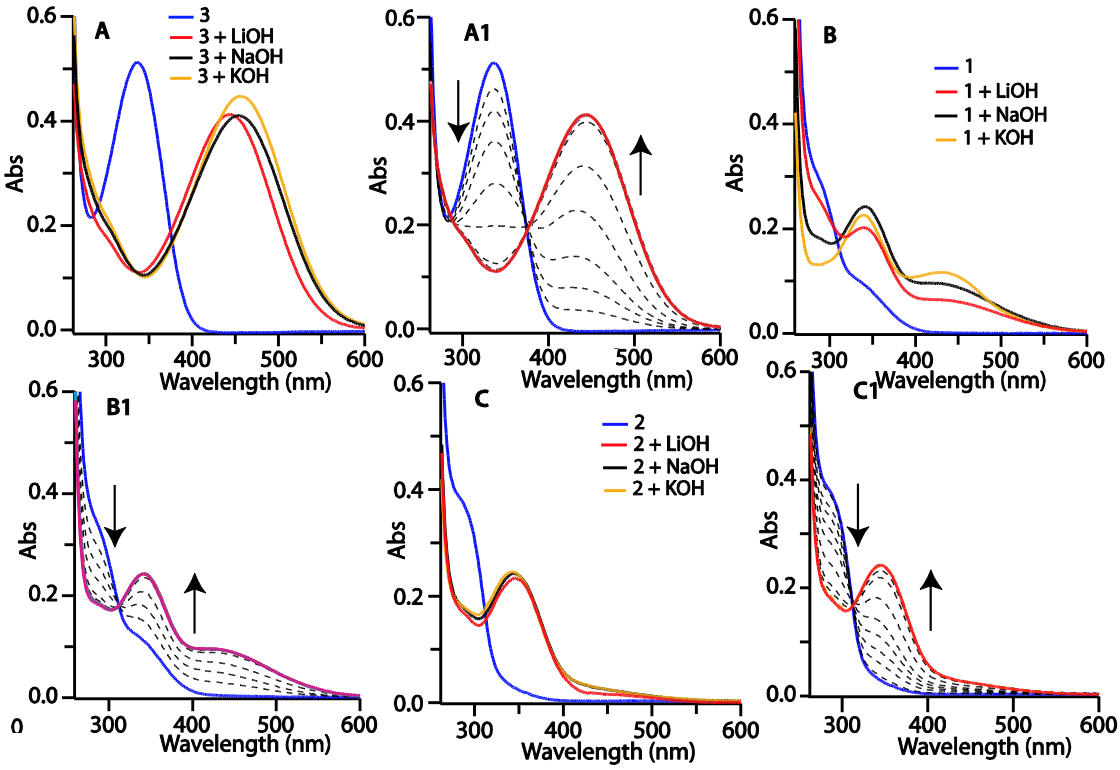

Figure 4.10 (A) UV-vis spectrum of **3** in DMSO absorbs at 337 nm (conc. $1x10^{-5}$ M) and upon treatment with LiOH/NaOH/KOH red shifted to 457/453/457 nm, respectively; (**A1**) UV-vis titration in DMSO **3** ($1x10^{-5}$M) *vs.* KOH ($1x10^{-3}$ M) shows the formation of CT complex. (**B**) 1 exhibited peak at 342 nm upon treatment with LiOH/NaOH/KOH red shifted to 443/442/449 nm, respectively, while (C) **2** (285 nm) red shifted to 345 nm in presence of LiOH/NaOH/KOH under similar conditions like **A**. **B1** and **C1** are titration between corresponding isomer and LiOH under similar conditions to **A1**.

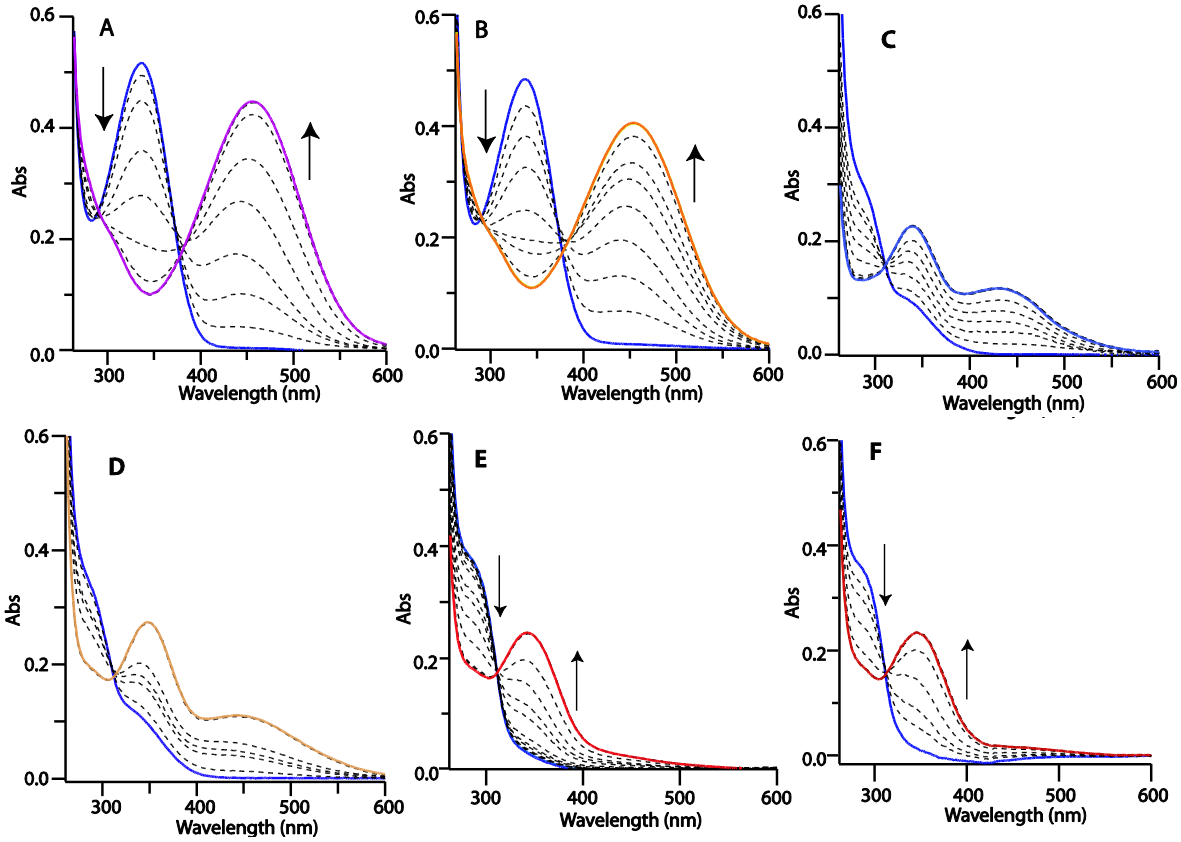

Figure 4.11 UV-vis titration of isomer **3** ($1x10^{-5}$ M) in DMSO (blue line), upon addition of aqueous solution of (conc. $1x10^{-3}$ M) (**A**) NaOH and (B) KOH shows the gradual decrease in absorbance at 337 nm and appearance of a new band at 457 nm through a nice isosbestic point at 377 nm. (**C** and **D**) UV-vis titration of isomer **1** ($1x10^{-5}$ M) in DMSO (blue line), upon addition of aqueous solution of (conc. $1x10^{-3}$ M) NaOH and KOH, respectively, shows the gradual decrease in absorbance at 292 nm and appearance of two new bands at 443 and 345 nm through a nice isosbestic point at 312 nm. The peak at 443 nm is because of the CT triggered by alkali base. The additional peak at 345 nm is because of the conformational change of gelator under the influence of alkali metal ion. (**E** and **F**) UV-vis titration of isomer **2** ($1x10^{-5}$ M) in DMSO (blue line), upon addition of aqueous solution of (conc. $1x10^{-3}$ M) NaOH and KOH, respectively, shows the gradual decrease in absorbance at 285 nm and appearance of a new band at 345 nm through a nice isosbestic point at 312 nm. The appearance of only one peak at 345 nm may be because of the conformational change in gelator under the influence of alkali base.

4.3.4 Intramolecular/Intermolecular CT

To avoid any artifact in the intramolecular or intermolecular CT, we strategically performed the aforementioned titration experiments with isomer **2**, and in turn very few bands in the CT region as well as a color change were observed (Fig. 4.10). The albeit weaker band in the CT

region of **2** + Li^+ suggests the presence of intramolecular CT in **3** + Li^+ and **1** + Li^+ rather than intermolecular CT. Furthermore, ICT is also theoretically not possible with the *meta* positioned $–NO_2$ group (Fig. 4.13 and Fig. 4.15).[22] However, the appearance of a new band at 345 nm may be because of the conformational change under the influence of alkali metal ions (Fig. 4.10). Remarkably, retention of the CT peak (~457 nm) also at huge dilution strongly supports the presence of intramolecular rather than intermolecular charge transfer (Fig. 4.12). However, a minor blue shift ($\Delta\lambda$ = 20 nm) in the CT band with dilution maybe due to the segregation of the gel network with the effect of dilution. Furthermore, variations of charge-transfer absorbance at 457 nm with concentration (dilution) follow the Beer–Lambert law, verifying the presence of ICT (Fig. 4.12).[20,21] In addition, TD-DFT calculations also support the presence of ICT in **3** + Li^+; the distribution of electron density was principally toward $–NO_2$ for the LUMO while close to the chiral center in the HOMO.[22] The energy required for the HOMO to LUMO transition was 3.06 eV comparable to CT transition (Fig. 4.12).[19] The significant increase in dipole moment of **3** before and after addition of Li^+ is 11.76 and 34.29 D, respectively, strongly confirming that Li^+ triggers ICT.[22] Apart from these, ligand **4** neither displays a color change nor a CT band after addition of Li^+ highlighting the positional significance as well as the role of the $–NO_2$ group in intramolecular charge transfer (Fig. 4.3).

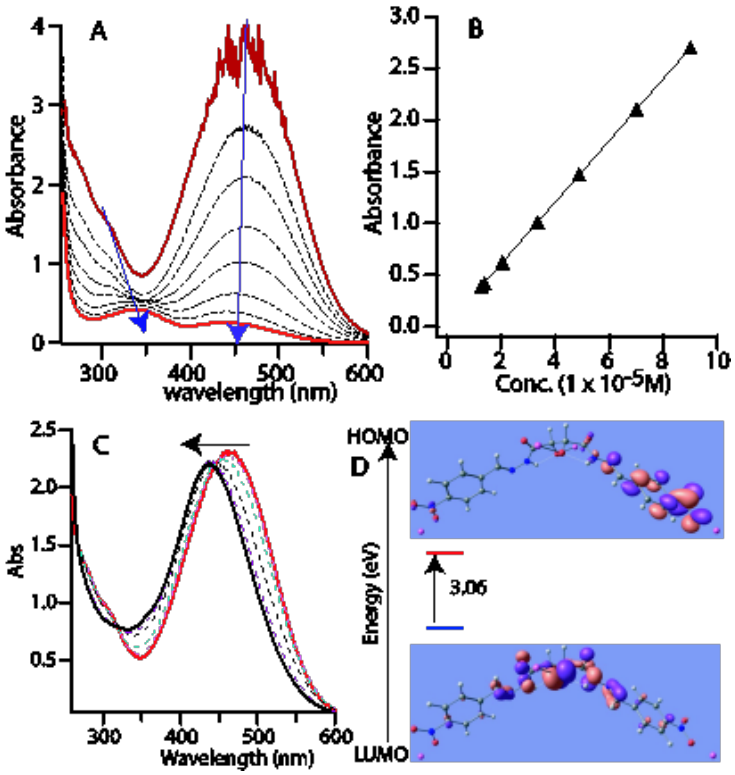

Figure 4.12 (A) UV-vis dilution experiment over **3**+Li^+, (B) The corresponding variation of absorbance upon varying the concentration, (C) UV-vis Variable temperature experiment over **3**+Li^+ in DMSO and (D) Energy gap between HOMO-LUMO of 3+Li^+.

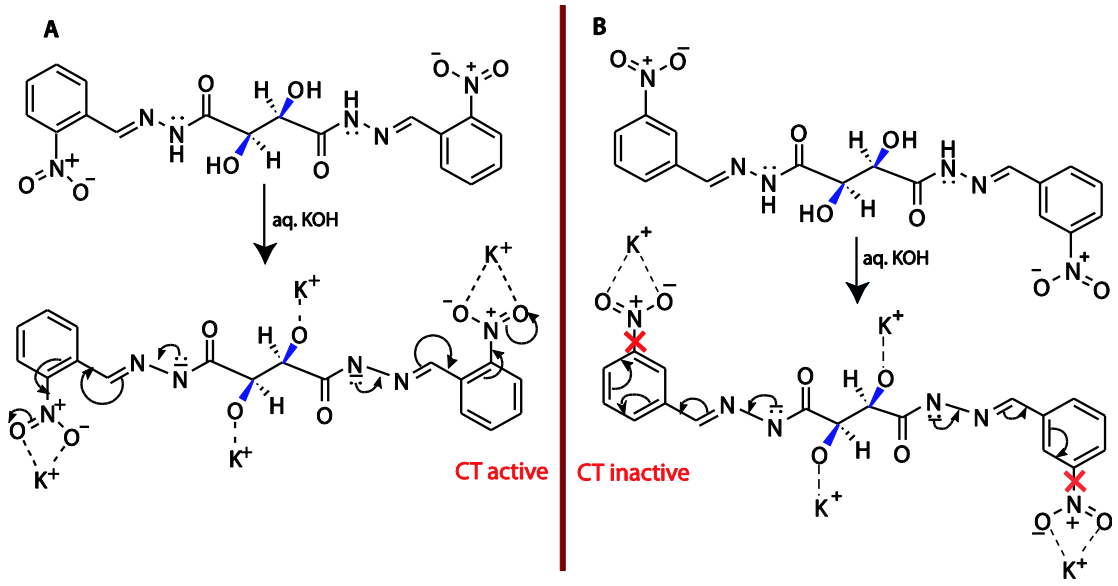

Figure 4.13 Plausible mechanism of presence and absence of charge transfer (A) isomer **1**+K^+ and (B) isomer **2**+K^+, respectively. The flow of charge density from amine N to $–NO_2$ group is feasible in case of isomer **1** and **3**, while in **2** does not because of lack of conjugative connectivity between ring and $–NO_2$ group.

4.3.5 Aggregation studies

Furthermore, to prove the CT followed by aggregation UV-vis and CD studies were performed using diluted gels. A variable temperature UV-vis experiment was performed on a diluted **3** + Li^+ gel (~$5x10^{-5}$ M; DMSO) in the temperature range of 25–90 °C. It was observed that an increase in temperature leads to an incessant blue shift ($\Delta\lambda$ = 25 nm) and this may be because of the deterioration of the CT as well as segregation (Fig. 4.12). Furthermore, the aforesaid blue shift was also observed in **3** + Li^+ and **1** + Li^+ acetonitrile containing diluted gels (Fig. 4.14). In addition, it also supports the observation made in color change upon heating and cooling (Fig. 4.2 and Video).Interestingly, variable temperature CD experiment on diluted **1** + Li^+ gel ($1x10^{-3}$ M; acetonitrile) displayed blue shift ($\Delta\lambda$ = 45 nm) for the peak corresponding to CT (393 nm) only while other peaks remain unaffected (Fig. 4.9). This observation strongly suggests the presence of a CT complex in the gel system. Dilution ($5x10^{-4}$ M) of the diluted **1** + Li^+ ($1x10^{-3}$ M) gel leads to a blue shift ($\Delta\lambda$ = 22 nm) of

the peak corresponding to CT only with a considerable decrease in the ellipticity of CD spectra proving segregation involving a CT complex (Fig. 4.9).

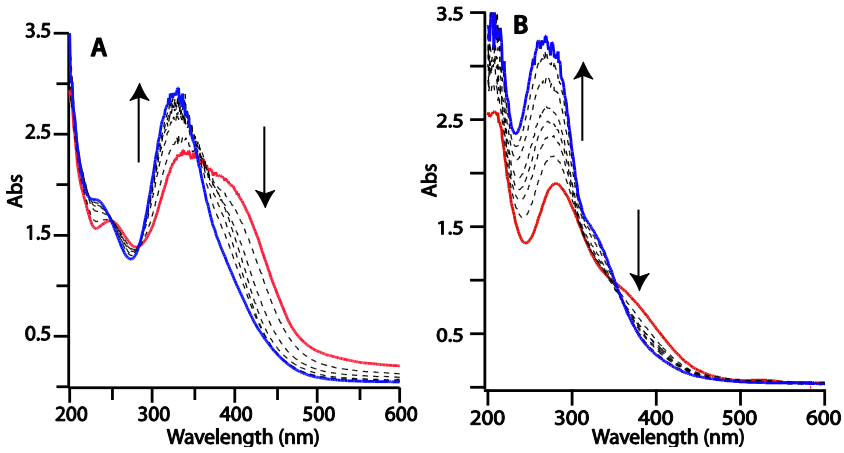

Figure 4.14 Spectral Variable temperature UV-vis experiment on diluted gel (~$5x10^{-5}$ M) shows the blue shift upon increasing the temperature from 30 –90 ºC (A) 3+Li^+ in acetonitrile; Δλ= 63 nm and (B) 1+Li^+ in acetonitrile; Δλ= 60 nm.

4.3.6 Mechanisms and the role of alkali metal ions in ICT

To elucidate the mechanism and role of alkali metal ions in aggregation as well as CT, UV-vis titration between CT complexes and [18]-crown-6 was carried out. Aliquot addition of [18]-crown-6 to the CT complex (**3** + K^+) resulted in successive decrease in the absorbance of the CT band (457 nm) and reappearance of a peak at 337 nm corresponding to isomer **3**through a good isosbestic point (377 nm) advocating the role of alkali metal ions in ICT (Fig. 4.15 and Fig. 4.16). Notably, the removal of the alkali metal ions with the help of [18]-crown-6 also causes a significant gradual blue shift ($\Delta\lambda$ = 22 nm), confirming the presence of aggregation with CT. Furthermore, to support the aforementioned experiment, an alkali base analogue, tetrabutylammonium hydroxide, added to solution in requisite proportions also exhibited the CT at 472 nm which was unaffected by excess [18]-crown-6 (Fig. 4.17). Based on these results, we could propose the plausible mechanism behind ICT in **3** and **1**. Alkali metal ions trigger the CT from deprotonated –NH to the $–NO_2$ group *via* π-conjugation

piloting the formation of a quinonoid structure (Fig. 4.15). This quinonoid structure is mainly responsible for intense color formation.[22] Furthermore, dilute acid treatment of the CT complex significantly blocked the charge transfer by protonation of the amine N and in the presence of alkali base activated the CT complex by deprotonation in a reversible manner (Fig. 4.16).[22] As the gelator is a symmetrical molecule it can thus be defined overall as the A–π–D-chiral-D–π–A type molecule. Remarkably, defiance of such conjugation in **2** and considerably depriving the electron-withdrawing ability of –COOH in **4** inhibits the charge transfer and gelation (Fig. 4.3 and 4.13). Thus, the ICT occurs through a 'pull–push' mechanism, where the alkali metal and base act as the pulling and the pushing agent, respectively.

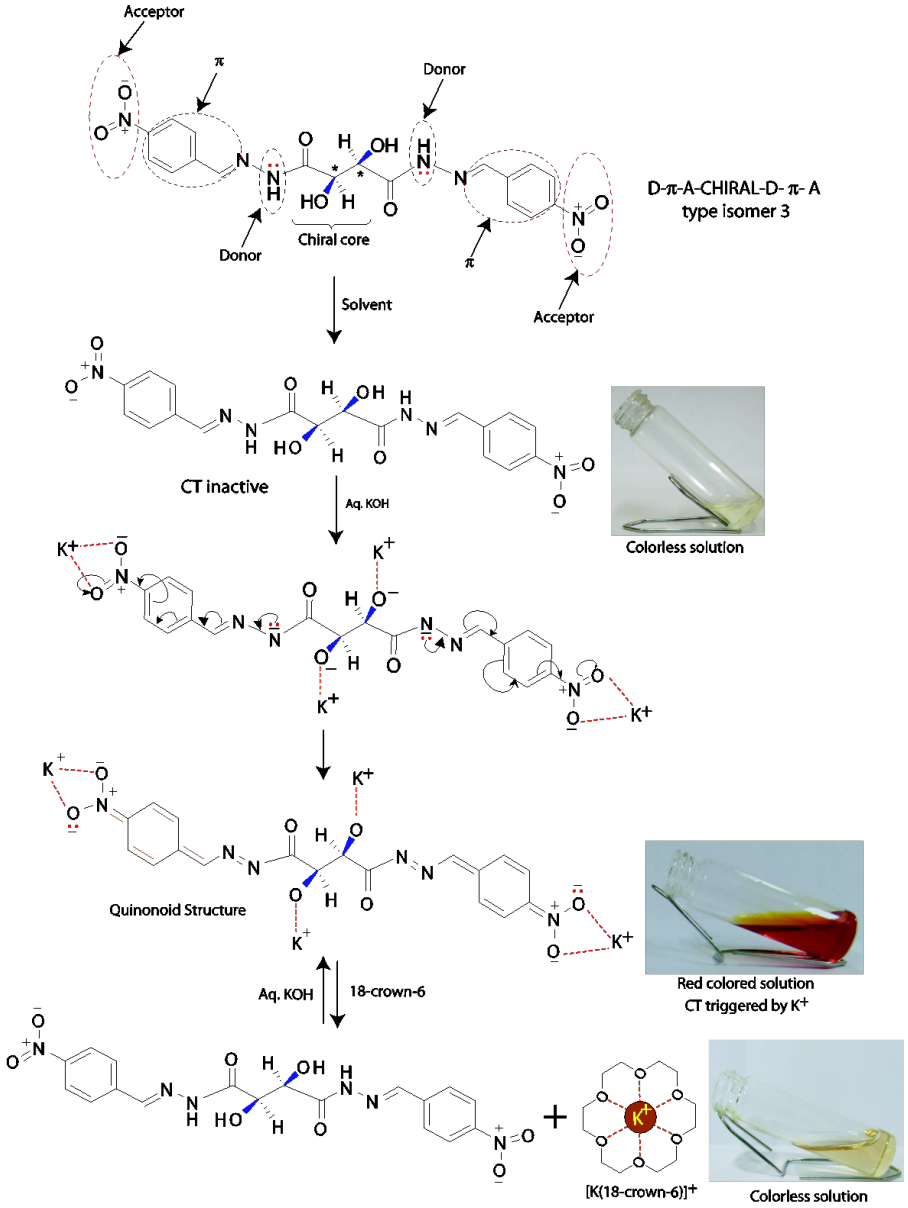

Figure 4.15 Plausible mechanism of charge transfer in symmetrical D–π–A based isomer 3 shows that the appearance of red color may be because of the formation of a quinonoid structure and the removal of the triggering effect K^+ with the help of [18]-crown-6 attains the original colorless solution as well as the structure in a reversible manner.

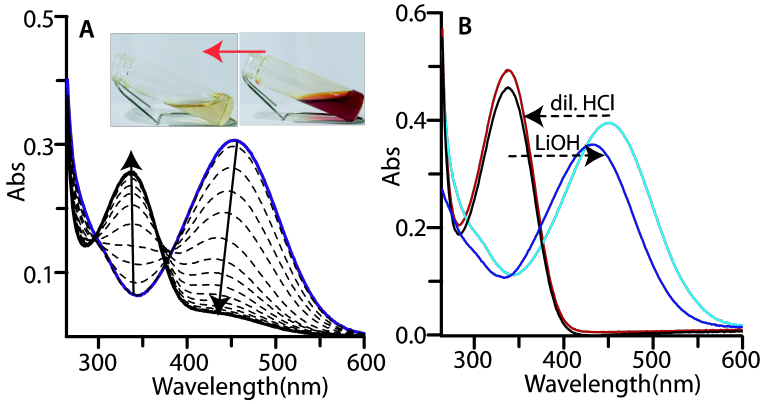

Figure 4.16 UV-vis titration spectra in DMSO (A) [**3** + K^+] *vs*. [18]-crown-6 demonstrate the removal of the triggering unit K^+, resulting the decrease in CT. The inset shows the color change. (B) The band corresponding to CT (**3** + K^+, DMSO, 457 nm, cyan colored line) shifted to 337 nm (red line) upon treatment with dilute HCl and upon further treatment with KOH achieved a peak corresponding to CT (blue line) in a reversible manner.

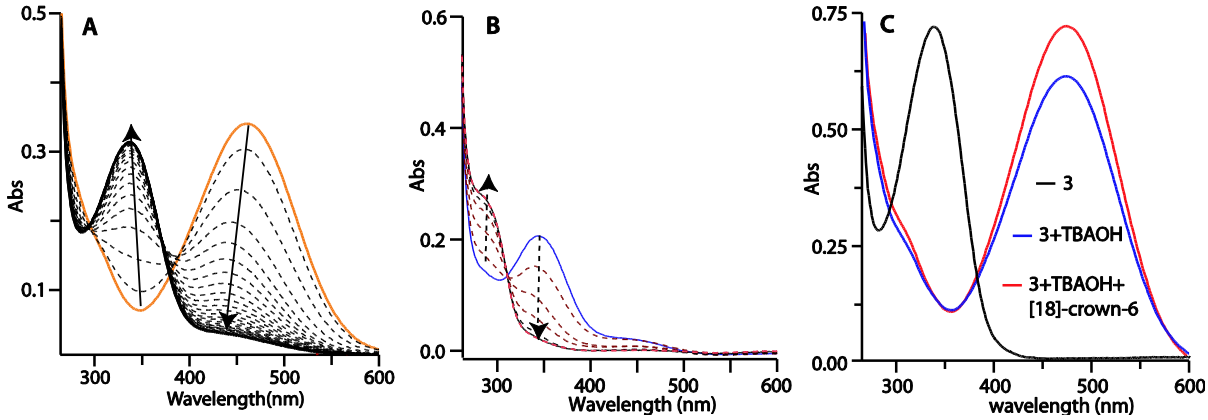

Figure 4.17 UV-vis titration experiments- (**A**) The band at 457 nm of **3**+Na^+ (yellow line, ~1x10^{-5} M, DMSO) corresponding to CT diminished upon treatment with [18]-crown-6 (1x10^{-3} M) and appeared a new peak simultaneously at 337 nm through a nice isosbestic point corresponding to isomer **3** demonstrate the removal of triggering unit Na^+, in turn, amputate the charge transfer. However, the consumption of [18]-crown-6 is more (~1.5 times) in case of **3**+Na^+ than **3**+K^+ may be because of the more selectivity of [18]-crown- 6 towards the K^+ than Na^+. (**B**) The band corresponding to isomer **2**+K^+ at 345 nm (blue line, 1x10^{-5} M, DMSO) shifted to 292 nm upon titration with [18]-crown-6 may be due to conformational reorganization in gelator upon removal of K^+. (**C**) Isomer **3** (337 nm) red shifted (473 nm, $\Delta\lambda$= 136 nm) upon addition of TBAOH and further there is no significant change observed upon treatment with excess [18]-crown-6.

4.3.7 ^{1}H NMR TITRATION STUDIES

To achieve clear mechanistic insights and also to have an idea about creation of the aggregates, ^{1}H NMR titration was carried out by taking **3** in d_6-DMSO (1.6x10^{-2} M) and LiOH in D_2O (1.0M). A neat spectrum of **3** was first recorded, which showed expected peaks for labile –NH, –OH protons as singlet at δ= 11.56 and 6.01 ppm, respectively, as well as aldemine H1 (N=CH) signal at δ = 8.58 ppm (Fig. 4.18). Furthermore, aromatic protons H2 appear as doublet at δ = 8.29 and H3 at δ = 7.93 ppm as well as chiral center protons H4 at δ = 4.54 ppm (Fig. 4.18). Furthermore, after five aliquot additions of LiOH (4.0 equiv.), it was observed that the protons significantly shifted up field in decreasing order of

$\Delta\delta$H1<$\Delta\delta$H4<$\Delta\delta$H2<$\Delta\delta$H3 (0.36, 0.25, 0.12 and 0.04 ppm). The unusual up field shift of protons for CT interactions has already been investigated.[7,8,20,21] The most pronounced effect seen for aldemine proton H1 can be rationalized in terms of establishment of strong interaction between aldemine H1 and the $-NO_2$ group of another molecule (Figure 4.18). Furthermore, a quite reasonable up field shift for H4 may be due to interaction of Li^+ with the neighboring oxo environment. Moreover, a significant shift of aromatic protons H2 adjacent to the $-NO_2$ group may be due to the effective interaction between Li^+ and the $-NO_2$ group. Upon achieving the 1:4 ratio of **3** and LiOH, broadening and loss of splitting patterns are observed, which can be ascribed to aggregation leading to gelation. The disappearance of signals corresponding to labile protons –NH and –OH may be due to the deprotonation by LiOH (Fig. 4.18).Thus, ^{1}H NMR titration studies undoubtedly suggest the involvement of aldemine protons as well as Li^+ interaction with $-NO_2$ and deprotonated oxo groups positioned at the chiral center, playing a crucial role in aggregation, and in turn, gelation.

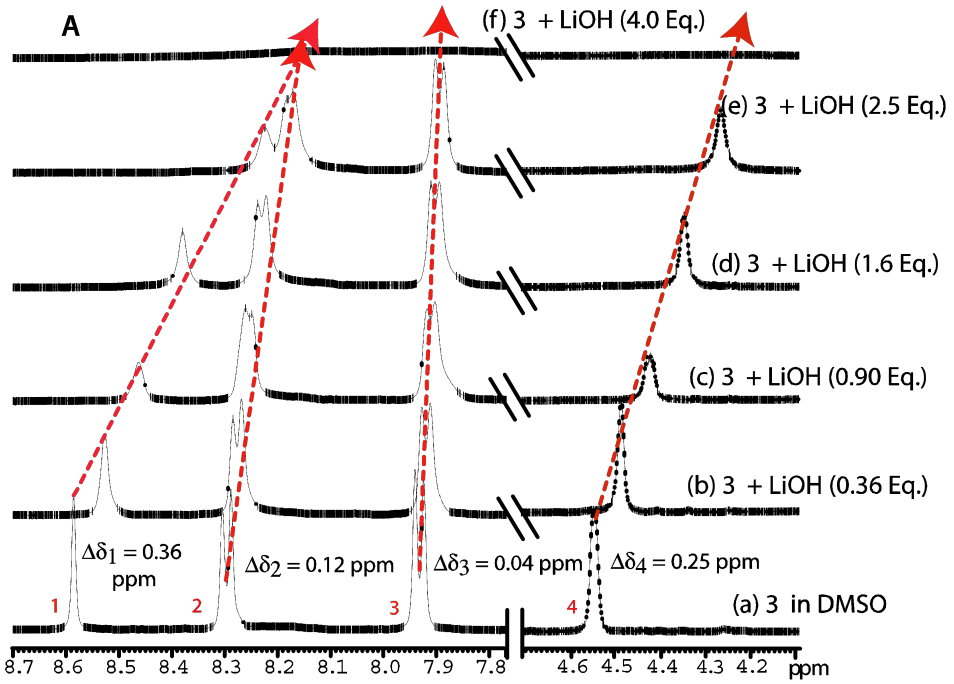

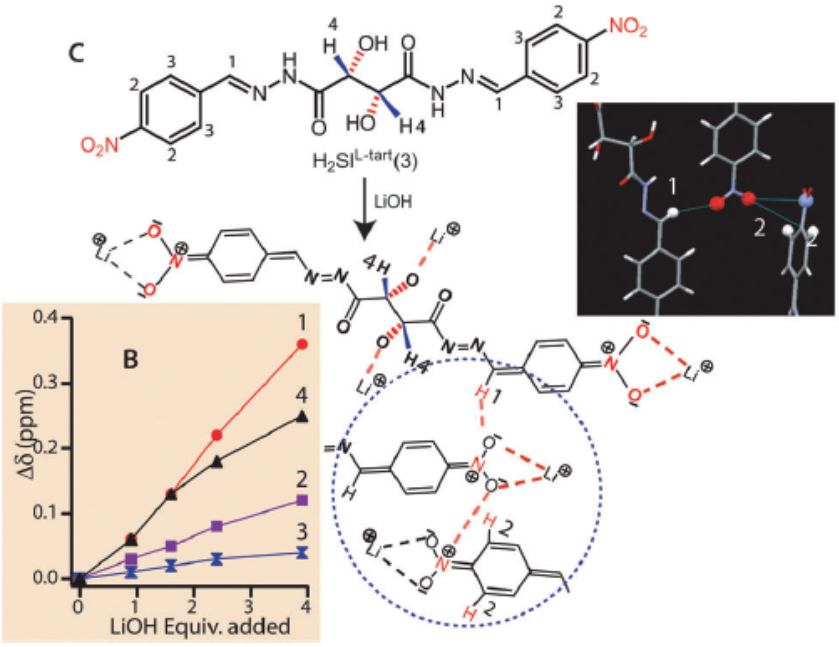

Figure 4.18 (A) ^{1}H NMR titration of **3** (500 MHz, DMSO-d_6, 300 K) with LiOH·H_2O; (a) free of Li^+ and (b)–(f) LiOH added up to 4 equivalents in 5 steps. The difference in chemical shift of a particular peak is mentioned at the bottom, (B) The plot between LiOH equivalent added and Δδ (ppm) clearly shows that the order of shift is ΔδH1 > ΔδH4 > ΔδH2 > ΔδH3 (0.36, 0.25, 0.12 and 0.04 ppm). (C) The proton labelling scheme and interactions elucidated from titration. The crystal structure well supports the observations made from ^{1}H NMR titration.

4.3.8 STRUCTURAL SUPPORT

The crystal of isomer **3** was isolated from the mixture of **3** and KOH in correct proportions (1:4) within 2–3 days.[17] It was surprising to see that **3** crystallizes without any K^+ ions in highly basic medium. The IR spectra of the crystals of **3** and a dried solution of **3** + K^+ also support the lack of interaction between K^+ and –NO_2 or –OH. Furthermore, the interaction stake place in the crystal lattice of **3** strongly supporting the observations made in ^{1}H NMR titration (Fig. 4.19). Powder X-ray diffraction data of dried gel (**3** + Li^+) show the amorphous nature while the peak patterns of **3** + Na^+ and **3** + K^+ impart the crystalline nature which matches nicely with the simulated crystallographic pattern (Fig. 4.20).[9] However, the

simultaneous crystallization of Na^+/K^+ carbonates cannot be ruled out.[10] The non-conductive nature of diluted gel (**3** + Li^+, $1x10^{-3}$ M) supports the non-electrolytic nature of gel. These results conclude that alkali metal ions trigger the CT temporarily, which upon solidification or aging of gel/solution disappears. Based on the results obtained from spectral, structural and morphological studies, we proposed a plausible mechanism behind gelation in Fig. 4.22.

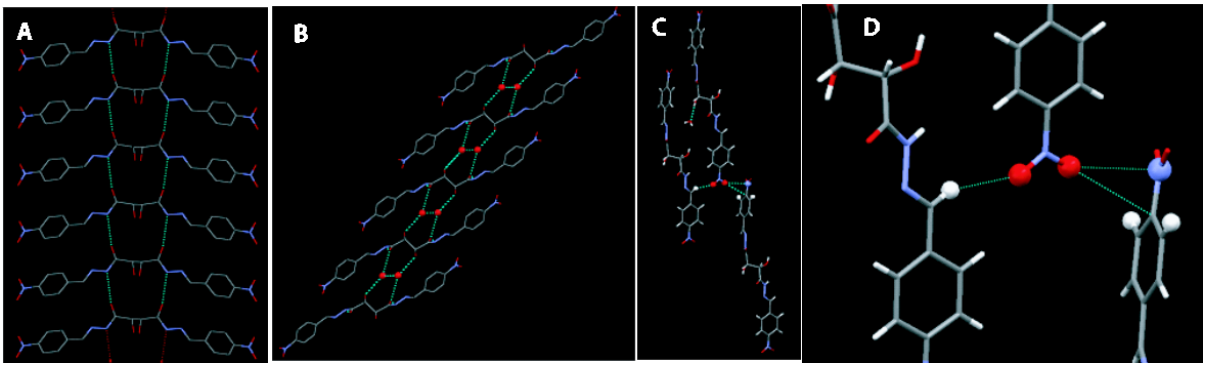

Figure 4.19 Crystal lattice of 3 (A) H-bonded lattice between NH and O along 'a' axis (NH33…O3, 4.884 Å), (B) Water molecules connect the two molecule of 3 in a fashion of three center two H-bond, (C) Role of $–NO_2$ group and aldemine proton in crystal packing and (D) in zoom image of C. The interactions shown in C and D have already been demonstrated in NMR titration experiment. (Crystallographic data and refinement parameters for 3: Empirical formula $C_9H_{10}N_3O_5$, Fw 240.20, T(K) 293(2), Wavelength 0.71073 (Å), monoclinic, C2, a = 15.791(3) Å, b = 5.0056(6) Å, c = 16.133(3) Å, $\alpha = \beta = 90$, $\gamma = 124.52(2)$, V = 1075.2(3) $Å^3$, Z = 4, ρcalcd = 1.484 Mgm^{-3}, $\mu = 0.123$ mm^{-1}, Reflections collected 1736, independent 1736, R1= 0.0554, wR2 = 0.1116 [$I>2\sigma$]; R1 = 0.0860, wR2 = 0.1324 [all data], GOF = 1.038, [3]Flack parameter = 0.23(3), CCDC 1445441. **H-bonds:** O5…H44 4.781 Å, O3…H33 4.884 Å, O3…H66 4.844 Å.

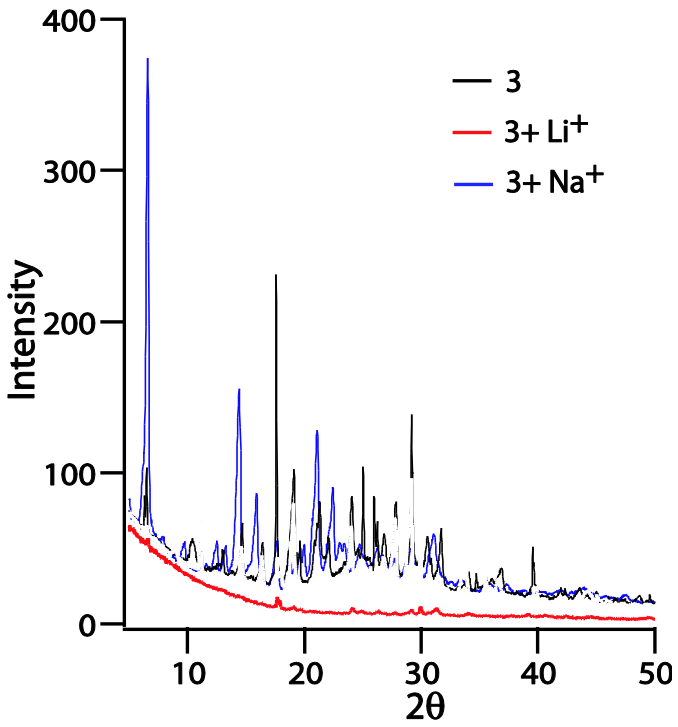

Figure 4.20 Powder X-ray diffraction pattern of gelator (isomer **3**, black line) and **3**+Li^+ (red line peaks) containing xerogel indicating amorphous nature of gel, while **3**+Na^+ (blue line) aggregate shows the crystalline nature in blue line. However, the formation of minor proportion of crystals of corresponding carbonates (Li^+/Na^+ absorbs atmospheric CO_2) and LiOH/NaOH cannot be ruled out.

4.12 Rheological properties

Rheological measurements were executed to scrutinize the mechanical and thermal stability of the freshly prepared metallogel (**3** + Li^+; acetonitrile) at a fixed concentration of 1% w/v (Fig. 9). The gel was directly subjected to the storage modulus (G') and loss modulus (G") measurement as a function of shear strain and stress at 25 ^oC and a frequency of 10 rad s^{-1}. The G' was found to be higher than the corresponding G" by ~1 order of magnitude, indicating the formation of a true gel phase material. Both G' and G" were almost independent of the applied strain below the 10% region and beyond this they cross each other at a point 17% indicating the phase transition of gel–sol. On the other hand, mechanical breakup of gel in applied stress was observed at a yield stress of 15 pa. Moreover, plots of G'

and G" values as a function of frequency (f) of the gel are independent of *f* at any given *f* in the experimental frequency region(-0.4 to 1.1 rad s^{-1}) and also G' is greater than G", suggesting the formation of a stable gel phase material.[2,23] The double logarithmic plot of complex viscosity (η*) *vs*. angular frequency(ω) reveals a gradient close to -1, which indicates constant declination of the viscosity with increasing frequency. Furthermore, thermal response of gel was monitored by a loss tangent(tan δ = G"/G') vs. temperature plot suggesting the critical temperature (T_{gel}) of the gel to be 84 ^{o}C.[10] Furthermore, phase transition at 84 ^{o}C for the acetonitrile containing gel is because of the evaporation of solvent from the gel network, in turn, collapsing the gel matrix. It is consistent with observations made from variable temperature UV-vis and CD studies. These results conclude that phase transition occurs *via* gel–solid, and propose the formation of a typical 'soft-solid like' gel phase material.[23]

4.4 CONCLUSIONS

In conclusion, three symmetrical chiral structural isomers (**1–3**) have been synthesized based on the A–π–D-chiral-D–π–A strategy. The alkali metal ion triggered ICT and gelation of these isomers have been established by various experiments. Excellent tuning of the morphology from ordinary to twisted fibers under the influence of alkali metal ions was supported by SEM and CD studies. Detailed UV-vis, ^{1}H NMR titration, crystal structure and DFT studies helped to elucidate the mechanism behind ICT involving gelation. Rheology supported the true gel phase material. The present findings may offer more efficient design toward ICT based metallogelators.

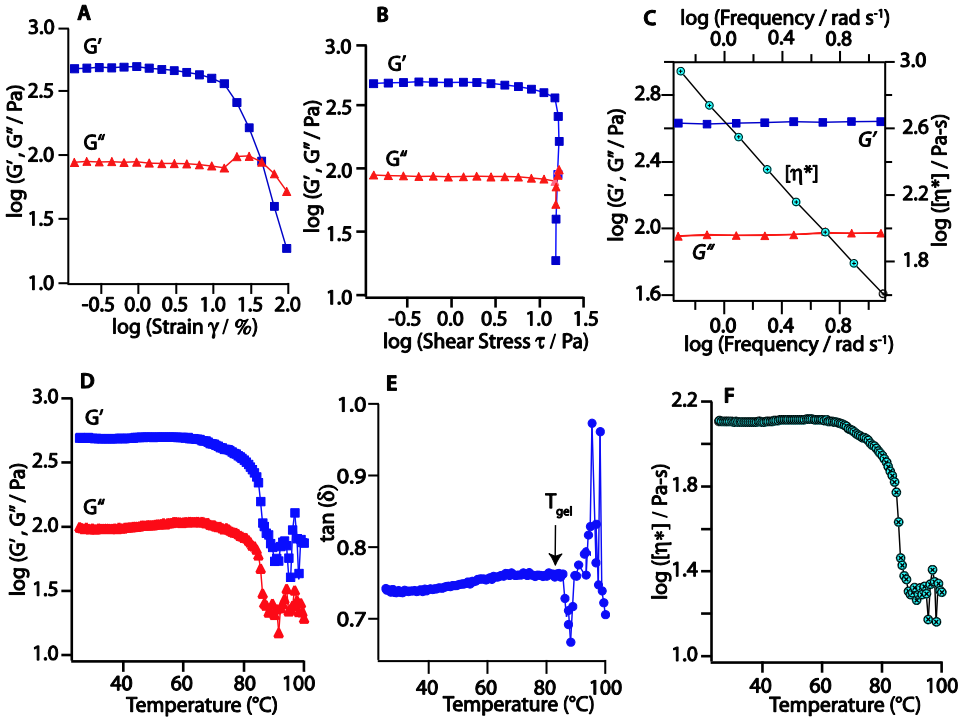

Figure 4.21 Rheological experiment on acetonitrile containing gel **3** + Li^+. (**A**) Dynamic oscillation strain sweep and (**B**) shear stress of G' and G" for CT gel, at frequency of 10 rad s^{-1} and 25 °C, and (**C**) primary axis: dynamic frequency sweep measurements of G' and G" at a strain of 0.5%. Secondary axis: complex viscosity measurements, (**D**) dynamic temperature ramps of G' and G", (**E**) Plot of the loss tangent (tan δ = G"/G') *vs.* Temperatue and (**F**) dynamic temperature ramp of complex viscosity measurement at 5 °C min^{-1}.

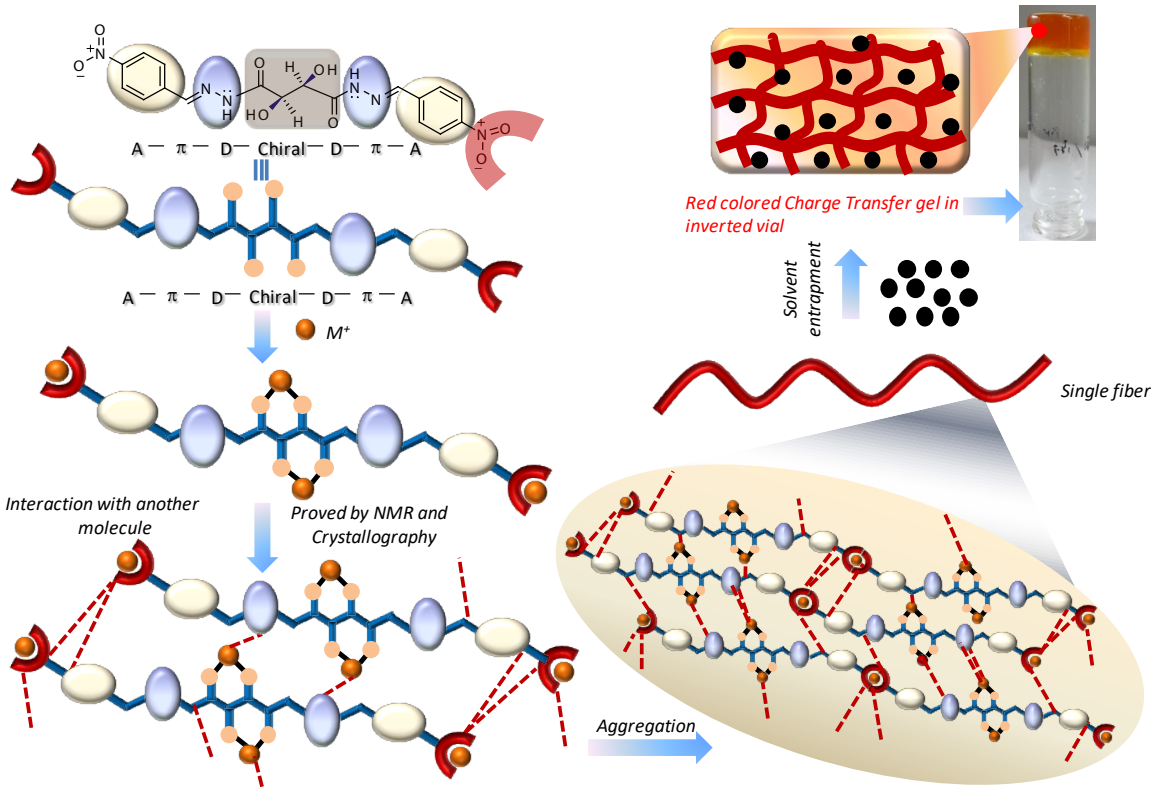

Figure 4.22 A pictorial representation of plausible mechanism of gelation.